

1 **Modeling demographic-driven vegetation dynamics and ecosystem biogeochemical cycling**
2 **in NASA GISS's Earth system model (ModelE-BiomeE v.1.0)**

3
4 Ensheng Weng^{1,2}, Igor Aleinov^{1,2}, Ram Singh^{1,2}, Michael J. Puma^{1,2}, Sonali S. McDermid³,
5 Nancy Y. Kiang², Maxwell Kelley², Kevin Wilcox⁴, Ray Dybzinski⁵, Caroline E. Farrior⁶,
6 Stephen W. Pacala⁷, Benjamin I. Cook²

7
8 ¹Center for Climate Systems Research, Columbia University, New York, NY 10025, USA

9 ²NASA Goddard Institute for Space Studies, 2880 Broadway, New York, NY 10025, USA

10 ³Department of Environmental Studies, New York University, New York, NY 10003, USA

11 ⁴Department of Ecosystem Science and Management, University of Wyoming, Laramie, WY
12 82071, USA

13 ⁵Institute of Environmental Sustainability, Loyola University Chicago, Chicago, IL 60660, USA

14 ⁶Department of Integrative Biology, University of Texas at Austin, Austin, TX 78712, USA

15 ⁷Department of Ecology & Evolutionary Biology, Princeton University, Princeton, NJ 08544 ,
16 USA

17

18 **Corresponding author:** Ensheng Weng (wengensheng@gmail.com; phone: 212-678-5585)

19

20 Submitted to **Geoscientific Model Development**

21

22

23 **Abstract:** We developed a new demographic vegetation model, BiomeE, to improve the
24 representation of vegetation demographic dynamics and ecosystem biogeochemical cycles in the
25 NASA Goddard Institute of Space Studies' ModelE Earth system model. This model includes the
26 processes of plant growth, mortality, reproduction, vegetation structural dynamics, and soil
27 carbon and nitrogen storage and transformations. The model combines the plant physiological
28 processes of ModelE's original vegetation model, Ent, with minor adaptations to fit the new
29 allometry and vegetation structure with the plant demographic and ecosystem nitrogen processes
30 represented from Geophysical Fluid Dynamics Laboratory's LM3-PPA. For global applications,
31 we added a new set of plant functional types to represent global vegetation functional diversity,
32 including trees, shrubs, and grasses, and a new phenology model to deal with seasonal changes in
33 temperature and soil water availability. Competition for light and soil resources is individual
34 based, which makes the modeling of transient compositional changes and vegetation succession
35 possible. BiomeE will allow ModelE to simulate long-term biogeophysical and biogeochemical
36 feedbacks between the climate system and land ecosystems. BiomeE simulates, with fidelity
37 comparable to other models, the dynamics of vegetation and soil biogeochemistry, including leaf
38 area index, vegetation structure (e.g., height, tree density, size distribution, crown organization),
39 and ecosystem carbon and nitrogen storage and fluxes. Further, BiomeE also allows for the
40 simulations of transient vegetation dynamics and eco-evolutionary optimal community
41 assemblage in response to past and future climate changes by incorporating core ecological
42 processes, including demography, competition, and community assembly.

43
44 **Key words:** Biogeochemical cycles, Eco-evolutionary optimality, Ecosystem modeling, Plant
45 traits, Vegetation dynamics

48 **1 Introduction**

49 Terrestrial ecosystems play a critical role in the climate system by regulating exchanges of
50 energy, moisture, and carbon dioxide between the land surface and the atmosphere (Sellers,
51 1997; Pielke et al., 1998; Meir et al., 2006). In turn, climate change has significantly affected
52 vegetation photosynthesis, water use efficiency, mortality, regeneration, and structure through
53 gradual changes in temperature and atmospheric [CO₂] together with shifts in climate extremes
54 (Brando et al., 2019; McDowell et al., 2020; Keenan et al., 2013; Huang et al., 2015). These
55 responses have triggered vegetation structural and compositional shifts. For example, global
56 forest mortality has increased in recent years (Allen et al., 2010; Anderegg et al., 2012), tree
57 sizes have decreased (Zhou et al., 2014; McDowell et al., 2020), and species composition has
58 shifted to more opportunistic species (Clark et al., 2016; Brodribb et al., 2020). The shifts in
59 vegetation function, composition, and structure can change the boundary conditions of the land
60 surface and affect the climate system (Nobre et al., 1991; Avissar and Werth, 2005; Garcia et al.,
61 2016; Green et al., 2017; Zeng et al., 2017). Realistic simulation of these processes is therefore
62 critical for Earth system models (ESMs).

63 The vegetation dynamics in ESMs are usually simulated using dynamic global vegetation
64 models (DGVMs) (Prentice et al., 2007), most of which are simplified in their representation of
65 ecological processes. The core assumptions of many vegetation models are a big-leaf canopy,
66 vegetation represented by only a few plant functional types (PFTs), single cohort-based
67 vegetation dynamics (“single-cohort” assumption, where the vegetation community at a land unit
68 are simulated as a collection of identical trees), lumped-pool-based biogeochemical cycles and
69 first order decay of soil organic matter. The competition of plant individuals and vegetation types
70 is approximately simulated as a function of productivity or Lotka-Volterra equations to predict

fractional PFT coverage (e.g., SDVGM, HYBRID, TRIFFID) (Friend et al., 1997; Woodward et al., 1998; Sitch et al., 2003). These simplifying assumptions make it possible to simulate the complex interactions of biological and ecological processes at the global scale.

These models are generally successful in reproducing land surface carbon, energy, and water fluxes after extensive tuning against data from sites, observational networks, and satellite remote sensing. However, the uncertainty of model predictions is high, and predictions can diverge substantially across different models (Friedlingstein et al., 2014; Arora et al., 2020). Lack of functional diversity and community assembly processes is one of the key issues in the vegetation modeling of ESMs, which makes the models unable to predict transient dynamics of vegetation composition and structure. A more mechanistic design that uses the fundamental principles of ecology to simulate the emergent properties of ecosystems for predicting ecosystem dynamics may therefore be necessary (Weng et al., 2017; Scheiter et al., 2013).

To this end, extensive efforts have been made to improve the representation of transient vegetation dynamics based on ecological theories and conceptual models. Two pivotal advances have been made in ecological vegetation modeling: 1) Demographic processes and trait-based representation of processes have been developed to improve the representation of functional diversity and size structure (Fisher et al., 2015; Weng et al., 2015; Pavlick et al., 2013) and 2) eco-evolutionary optimal and game theoretical approaches have been proposed to predict the flexibility of parameters and processes (McNickle et al., 2016; Weng et al., 2017). These concepts are mainly applied in modeling photosynthesis (Wang et al., 2017; Prentice et al., 2014), allocation (Farrior et al., 2013; Dybzinski et al., 2015), and evolutionarily stable strategy (ESS) of plant traits (Falster et al., 2017; Weng et al., 2017). These ideas for incorporating

93 ecological and evolutionary principles into ESMs have been summarized in several recent review
94 papers (Harrison et al., 2021; Franklin et al., 2020; Kyker-Snowman et al., 2022).

95 There are still major challenges to integrating these more sophisticated ecological modeling
96 approaches into the complex land models of ESMs, where the explicit simulations of energy,
97 water, and carbon fluxes at high frequencies are required for interacting with the atmosphere and
98 climate system. The details of vegetation dynamics, including the key functions from leaf
99 photosynthesis, respiration, biogeochemical fluxes between pools, demographic processes,
100 community assembly, vegetation structure, and competition output, must be well-organized
101 hierarchically and computed efficiently (Fisher and Koven, 2020; Franklin et al., 2020).
102 Representing these processes in ESMs, however, can complicate model structure and behavior,
103 especially for the interaction between physiology and vegetation composition, and cause large
104 increases in the computational burden. Thus, the implementation of detailed vegetation
105 demographic processes and size categories into ESMs would benefit from more parsimonious
106 approaches, such as is the case for the Robust Ecosystem Demography model (Argles et al.,
107 2020).

108 Including highly complex processes does not necessarily increase model predictive skills
109 (Famiglietti et al., 2021; Forster, 2017; Hourdin et al., 2017). On the contrary, it may greatly
110 obscure model transparency and increase uncertainty, and positive feedbacks in these processes
111 may result in large and unanticipated shifts of vegetation states. Any small differences in model
112 setting or even parameter differences can result in distinct predictions, especially in vegetation
113 structure, which is supposed to be predicted by these types of models. These processes make
114 demographic vegetation models often unreliable when compared to the well-tuned “single-
115 cohort” vegetation models that simplify the reproduction and mortality as growth and turnover of

116 continuous biomass pools. Additionally, the long history of land models and the requirements of
 117 backward compatibility (i.e., reversing the model to its previous functions) mean developers
 118 must often build their new functions on top of previous modeling assumptions and coding
 119 structure (Fisher and Koven, 2020), adding up to multiple adjustments of previous processes and
 120 making the model untraceable.

Deleted: legacy

Deleted: technical

Deleted: reversibility in model development

Deleted: their

Deleted: model

Deleted: on top of

Deleted: assumptions

121 To explicitly model the transient dynamics of ecosystems in ESMs while preserving model
 122 traceability, we need clear assumptions, detailed physical processes, and traceable model
 123 structure. For the best chance of accurate predictions outside of the model's testing data, model
 124 processes should be based on the fundamental biological and ecological principles to predict
 125 ecosystem emergent properties, instead of fitting the emergent patterns directly as many models
 126 do currently. To achieve this, we need to properly represent the tradeoffs of plant traits, balance
 127 the complexity of the model structure and priority for the processes that are required by the
 128 general circulation model (GCM), and also make model assumptions transparent and processes
 129 robust. These requirements make it difficult to fully implement the modeling approaches that are
 130 well-developed in the ecological modeling community.

131 This paper describes a vegetation demographic and soil organic decomposition model that
 132 is incorporated into the NASA Goddard Institute for Space Studies (GISS) Earth system model,
 133 ModelE. Our goal is to develop a parsimonious, transparent model that 1) allows ModelE to
 134 simulate the ecological dynamics of terrestrial ecosystems and vegetation at the global scale and
 135 2) sets up a modeling framework for solving some of the major challenges for incorporating
 136 important ecological mechanisms into ESMs. For (1), we have incorporated core ecosystem
 137 processes, including plant growth, demography, community assembly, and ecosystem carbon and
 138 nitrogen cycles. For (2), we have developed PFTs that are plant trait-based and a competition

Deleted: The NASA Goddard Institute for Space Studies' Earth system model, ModelE, has a land model for representing land surface hydrology (TerraE) (Rosenzweig and Abramopoulos, 1997; Schmidt et al., 2014) and a vegetation biophysics scheme (from the Ent Terrestrial Biosphere Model)(Ito et al. 2020; Kelley et al. 2020; Schmidt et al. 2014), with fixed vegetation traits (e.g., leaf mass per area, C:N ratio), fixed biomass, canopy height, and plant density, and seasonal leaf area index prescribed from a satellite-derived data set (Ito et al., 2020). The Ent TBM calculates canopy radiative transfer (Friend & Kiang 2005), canopy albedo, canopy conductance, photosynthesis, autotrophic respiration, and some phenological behaviors of leaf biophysics (Kim et al., 2015). The carbon allocation scheme of Kim et al. (2015) is used in ModelE with prescribed canopy structure and LAI, routing the carbon that would otherwise be allocated to plant tissues via growth instead directly as litter into soil carbon pools, thus conserving carbon for fully coupled carbon cycle simulations, but resulting possibly in imbalanced plant carbon reserve pools where the prescribed canopy structure is not in equilibrium with the simulated climate (Ito et al., 2020)....

Deleted: ¶

Deleted: parsimonious

Deleted: can be

Deleted: GISS ModelE ESM.

187 scheme that is individual-based. In this paper, we describe this model in detail, and evaluate its
188 performance compared to both observations and other state-of-the-art DGVMs.

189

190 2 Model Description

191 2.1 GISS ModelE and BiomeE Overview

192 ModelE has a land model for representing land surface hydrology (TerraE) (Rosenzweig and
193 Abramopoulos, 1997; Schmidt et al., 2014) and a vegetation biophysics scheme (from the Ent
194 Terrestrial Biosphere Model; TBM) (Ito et al. 2020; Kelley et al. 2020; Schmidt et al. 2014),
195 with fixed vegetation traits (e.g., leaf mass per area, C:N ratio), fixed biomass, canopy height,
196 and plant density, and seasonal leaf area index prescribed from a satellite-derived data set (Ito et
197 al., 2020). The Ent TBM calculates canopy radiative transfer (Friend & Kiang 2005), canopy
198 albedo, canopy conductance, photosynthesis, autotrophic respiration, and some phenological
199 behaviors of leaf biophysics (Kim et al., 2015). The carbon allocation scheme of Kim et al.
200 (2015) is used in ModelE with prescribed canopy structure and LAI, routing the carbon that
201 would otherwise be allocated to plant tissues via growth instead directly as litter into soil carbon
202 pools, thus conserving carbon for fully coupled carbon cycle simulations, but resulting possibly
203 in imbalanced plant carbon reserve pools where the prescribed canopy structure is not in
204 equilibrium with the simulated climate (Ito et al., 2020).

205 BiomeE is a standalone simulator derived from the LM3-PPA (Weng et al., 2015). It is a
206 demographic vegetation model that simulates plant physiology, vegetation demography, adaptive
207 dynamics (eco-evolutionary adaptation), and ecosystem carbon, nitrogen, and water cycles (Fig.
208 1) (Weng et al., 2017, 2019). In this model, the PFTs are defined by a set of combined plant
209 traits with their values sampled from the observed ranges to represent a specific plant type.

Deleted:

Deleted: Structure and

Formatted: Font: Bold

Deleted: ; TBM

Deleted: a PFT is

Individual plants are categorized into cohorts and arranged in different vertical canopy layers according to their height and crown area following the rules of the Perfect Plasticity Approximation model (PPA, Strigul et al., 2008). Sunlight is partitioned into canopy crown layers according to Beer's law. The cohort is the basic unit to carry out physiological and demographic activities, e.g., photosynthesis, respiration, growth, reproduction, mortality, and competition with other individuals.

Deleted: The individual is the basic unit to carry out physiological and demographic activities, e.g., photosynthesis, respiration, growth, reproduction, mortality, and competition with other individuals.

Deleted: With the PPA model, a key parameter for light competition, the height of canopy closure (i.e., critical height, ...H

Deleted: H

Deleted: *, is defined; all the plants above this context-dependent height get full sunlight and all trees below this height are shaded by the upper layer trees.

Deleted:

Formatted: Centered, Line spacing: Double

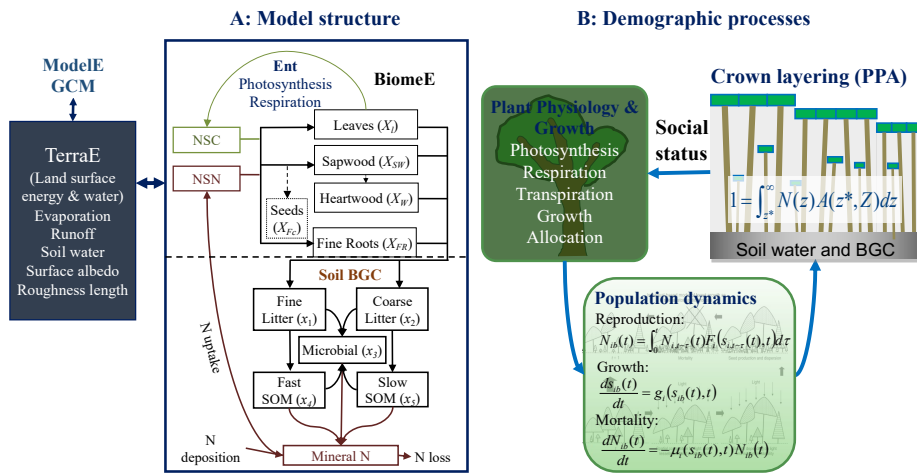


Figure 1 Schematic diagram of the coupling of BiomeE into ModelE

Panel A shows the structure of carbon and nitrogen pools and fluxes, and the interactions of BiomeE with TerraE, the land surface model in ModelE. The lines are the flows of carbon (green), nitrogen (brown), and coupled carbon and nitrogen (black). The green box is for carbon only. The brown boxes are N pools. The black boxes are for both carbon and nitrogen pools. The C:N ratios of leaves, wood, fine roots, and microbes are fixed and those of litters and SOM pools are dynamic with input and output. Panel b shows the demographic processes of BiomeE and the key processes of population dynamics.

244 The demographic processes generate and remove cohorts and change the size and density of
 245 plant individuals in the cohorts. With explicit description of cohort size, organization, and
 246 composition during a model run, the model simulates competition for light and soil resources,
 247 community assembly and vegetation structural dynamics. These processes are hierarchically
 248 organized in this model and run at various time steps: half-hourly or hourly for plant physiology
 249 and soil organic matter decomposition, daily for growth and phenology, and yearly for
 250 demography.

251 We coupled the standalone BiomeE into ModelE's land model for simulating global
 252 dynamics of vegetation and biogeochemical cycles and their feedback to the climate system. For
 253 extending this model to the global scale, we designed a new set of PFTs to represent the
 254 functional diversity of global vegetation and a new phenological scheme to deal with
 255 temperature and water seasonality. Leaf photosynthesis processes are taken from ModelE's
 256 existing vegetation model, Ent (Kim et al. 2015), and used to calculate the carbon budget that
 257 drives vegetation dynamics. Plant growth and demographic processes and the soil organic matter
 258 decomposition and nitrogen cycle processes are from BiomeE (Fig. 1). The land surface energy
 259 and water fluxes are calculated by TerraE with land surface characteristics jointly defined by the
 260 vegetation model.

261 **Plant functional types**

262 In this model, we use a set of continuous plant traits to define plant functional types, so that we
 263 can simulate plant emergent properties (such as dominant plant types, vegetation compositional
 264 changes, etc.) in response to climate changes based on the underlying plant physiological
 265 properties and ecological principles through eco-evolutionary modeling in the future. For
 266 example, life forms are defined by the continuums characterized by wood density (woody vs.

Deleted: s

Deleted: extendingextrapolating

Deleted:

Deleted:

Deleted: environmental

Deleted: temperature and water

Deleted: .

Deleted: taken

Deleted:)

Deleted: , and used to calculate the

Deleted: , for calculating

herbaceous), height growth coefficient (tree vs. shrub), and leaf mass per unit area (LMA, for evergreen vs. deciduous). Deciduousness is defined by cold resistance (evergreen vs. cold deciduous), and drought resistance (evergreen vs. drought deciduous). Grasses are simulated as tree seedlings with all stems senescent along with leaves at the end of a growing season. The individuals are reset back to initial size each year and the population density is also reset using the total biomass of current cohort and predefined initial size of grasses. The photosynthesis pathway is predefined as C3 or C4.

We defined 9 PFTs for our test runs in this paper to roughly represent global vegetation functional diversity (Table 1) according to their life form (tree, shrub, and grass), photosynthesis (C3 and C4), and leaf phenology (evergreen and deciduous).

Table 1 Plant functional types used in BiomeE

Plant functional types	V_{cmax}	LMA (kg C m ⁻²)	ρ_w (kg C m ⁻³)	α_z	$T_{0,c}$	$\beta_{0,D}$	PS pathway
1. Tropical evergreen broadleaf	18	0.07	360	30	15	0	C ₃
2. Temperate/boreal evergreen needleleaf	18	0.14	300	30	-80	0	C ₃
3. Temperate/boreal deciduous broadleaf	22	0.025	350	30	15	0	C ₃
4. Tropical drought deciduous broadleaf	20	0.03	250	30	15	0.2	C ₃
5. Boreal deciduous needleleaf	20	0.03	300	30	15	0.0	C ₃
6. Cold shrub	18	0.025	360	20	15	0.1	C ₃
7. Arid shrub	18	0.03	360	20	15	0.1	C ₃
8. C3 grass	20	0.025	90*	10	5	0.2	C ₃
9. C4 grass	15	0.025	90*	10	5	0.2	C ₄

LMA: leaf mass per unit area, ρ_w : wood density, α_z : Height coefficient, $T_{0,c}$: Critical temperature for phenology offset, $\beta_{0,D}$: critical soil moisture index for the offset of phenology, PS: photosynthesis pathway, E: evergreen, C: cold-deciduous, D: drought-deciduous. *Grass stem density is calculated as tissue biomass divided by stem volume. The tissue density of grass's stems is as high as wood.

Formatted: Font: Not Bold

Deleted:

Deleted: ¶
Plant functional types

Deleted: ¶

Deleted: ¶

Deleted: α_H

301

302 All PFTs go through the same set of plant physiological and demographical processes in
303 the model and derive different emergent properties due to the differences in parameters, rather
304 than differences in processes (except C₃ and C₄). With these different strategies, they have their
305 advantages and risks in different environments. An advantage of this continuous parameter
306 design is that one PFT can switch to another by changing its parameters (except C₃ and C₄
307 photosynthesis pathways). This opens the way for eco-evolutionary and ecological community
308 assembly simulation to explore the competitively optimal plant traits as environments change.

309 Phenology

310 Phenology types are defined by two parameters, a critical low temperature and a critical soil
311 moisture index, that are used to trigger leaf fall. These two parameters define 4 phenological
312 types with their possible factorial combinations: evergreen, drought-deciduous, cold-deciduous,
313 and drought-cold-deciduous. Evergreen PFTs have high resistances to cold (i.e., very low critical
314 temperature) and drought (very low soil drought). Cold and drought deciduous PFTs have low
315 critical temperature and soil drought index, respectively. These phenological types represent
316 different strategies of dealing with environmental stresses and pressure of competition. It is
317 possible that the evergreen would be more competitive in high seasonality regions (e.g.,
318 evergreen in boreal regions), though the first response of plants to harsh environments (e.g., cold
319 or dry) is to shed their leaves. Our definition of phenology is designed to make it possible to
320 evaluate the competitively optimal strategy in future studies.

321 For the cold-deciduous PFTs (3 and 5), we used the growing degree days above 5 °C
322 (GDD₅) to control the timing of phenological onset and a critical low temperature (T_m) to control
323 the offset. GDD₅ is calculated from the days that temperature starts to increase from the coldest

Deleted:

Deleted:

326 days in the non-growing season. The critical value of GDD that the plants require for growth
 327 (GDD_c) is defined as a function of chilling days in the non-growing season (Prentice et al.,
 328 1992):

$$GDD_c = a_0 + d \cdot e^{-b \cdot N_{CD}}, \quad (1)$$

329 where, N_{CD} is the days of the cold period in nongrowing season before bud burst, a_0 is the
 330 minimum GDD_c (50) when the cold period is sufficiently long, d is the maximum addition of
 331 GDD_c (800) when there is no cold period (i.e., $N_{CD}=0$), b is a shape coefficient (0.025). These
 332 parameters are tunable and should change with acclimate to new climates.

333 The running mean temperature that represents the mean temperatures over a short period of time
 334 is calculated as:

$$\begin{cases} T_m(i) = T_d(i), & \text{when } i = 1 \\ T_m(i) = 0.8T_m(i-1) + 0.2T_d(i), & \text{when } i \geq 2 \end{cases} \quad (2)$$

335 We used an index of cold condition (accumulative low temperature, ALT) to make sure the low
 336 temperature signal is persistent and differentiates the signal of the seasonal temperature changes
 337 and the stochastic low temperature stresses in growing seasons. The critical temperature for
 338 triggering leaf senescence (T_c) is calculated as a function of the number of growing days (N_{GD}).

$$T_c = T_{0,c} - s \cdot e^{-c \cdot (\max(0, N_{GD} - L0))}, \quad (3)$$

339 where, $T_{0,c}$ is the highest critical temperature when N_{GD} is sufficiently long, s is the range that a
 340 critical temperature can change, c is a shape parameter, $L0$ defines the lowest critical temperature
 341 ($T_{0,c} - s$) when N_{GD} is smaller than $L0$. The rationale in this equation is that when a growing
 342 period is not long enough, plants need a lower T_c to trigger leaf fall so that they can have a

growing season that is not too short. This setting is based on the thermal adaptation analysis of Yuan et al. (2011).

For the drought deciduous PFTs (tropical drought deciduous broadleaf, arid shrub, C₄ grass), we used a soil moisture index (s_D) to ~~start~~ and ~~end~~ a growing season.

$$s_D = \sum_{i=1}^n \text{Min} \left(1.0, \max \left(\frac{\theta_i - \theta_{WP,i}}{\theta_{HC,i} - \theta_{WP,i}}, 0.0 \right) \right), \quad (4)$$

where i is the soil layer in root zone, θ is soil water content (vol/vol), θ_{WP} is wilting point, and θ_{HC} is soil water holding capacity. ~~The critical soil moisture values that trigger new leaf growth and leaf fall are defined as PFT-specific parameters. We slightly tuned these two parameters according to the soil moistures where the deciduous PFTs' leaves start to grow or fall. Usually, the critical soil moisture for starting new leaf growth is higher than the soil moisture levels that trigger leaf fall so that the plants can have a stable growing season.~~

Plant demography and biogeochemical cycles

Allometry and Plant architecture

~~The plant allometry and architecture are critical for plant resources allocation, light capture, and soil water and nutrients uptake. The allometry equations are the same as those used in LM3-PPA~~ (Weng et al., 2015; Farrior et al., 2013);

$$\begin{cases} A_C = \alpha_C D^{\theta_C} \\ Z = \alpha_Z D^{\theta_Z} \\ S = 0.25\pi\rho\Lambda\alpha_H D^{2+\theta_H}, \\ A_L^* = l_{max} A_C \\ A_{FR}^* = \varphi_{RL} l_{max} A_C \end{cases} \quad (5)$$

where D is tree diameter; A_C is crown area; Z is tree height; S is ~~woody~~ biomass (sapwood plus heartwood); α_C and α_Z are the scaling factors for crown area and plant height, respectively; θ_C ,

Deleted: initiate

Deleted: terminate

Deleted: The critical soil moisture values that trigger new leaf growth and leaf fall are defined as PFT-specific parameters. evergreen PFTs having low θ^* .

Deleted: The allometry of woody PFTs follows the equations used in LM3-PPA

Deleted: . Plant allometry is described by the following equations...

Deleted: ¶

Deleted: structural

Deleted: ,

Deleted:

Deleted: ,

377 ~~and~~ θ_z are the ~~exponents~~ for crown area and tree height, respectively; π is ratio of a circle's
 378 circumference to its diameter; ρ is wood density (kg C m^{-3}); A is the taper factor from a cylinder
 379 to a tree with the same D ; A_L^* and A_{FR}^* are the ~~target~~ surface area of leaves and fine roots,
 380 respectively; ϕ_{RL} is the area ratio of leaves to roots. l_{\max} is ~~the maximum~~ leaf area per unit
 381 crown area, defined as a function of plant height (Z):

$$l_{\max}(Z) = L_{\max,0}(Z + h_0)/(Z + H_0), \quad (6)$$

382 where $L_{\max,0}$ is the maximum crown LAI when a tree is sufficiently tall, Z is tree height, h_0 is a
 383 small number that makes a minimum $l_{\max}(L_{\max,0}(h_0/H_0))$ when tree height is close to zero, and
 384 H_0 is a curvature parameter.

385 Plant growth and allocation of carbon and nitrogen to plant tissues

386 The allocation of NPP wood, leaves, and roots is affected by climate and forest age (Xia et al.,
 387 2019; Litton et al., 2007). However, vegetation models cannot capture these patterns well at large
 388 spatial scales, even if the adaptive responses to climate and forest ages are considered (Xia et al.,
 389 2019, 2017), partly because of the absence of explicit representation of shifts in species
 390 composition and competition between individuals (Dybzinski et al., 2015; Franklin et al., 2012).
 391 BiomeE has an optimal growth scheme that drives the allocation of carbon and nitrogen to
 392 leaves, fine roots, and stems based on the optimal use of resources and light competition (Weng
 393 et al., 2019). In this scheme, the growth of new leaves and fine roots follows the growth of
 394 woody biomass (i.e., stems), and the area ratio of fine roots to leaves is kept constant during the
 395 growing season. The allocation of available carbon between structural (e.g., stems) and
 396 functional (e.g., leaves and fine roots) tissues is optimal for light competition at given nitrogen
 397 availability.

Deleted:

Deleted: ,

Deleted: allometry parameters

Deleted:

Deleted:

Deleted: potential

Deleted:

Deleted: (i.e., potential crown LAI)

Deleted: H

Formatted: Font: Italic

Mathematically differentiating the stem biomass allometry in Eq. 5 with respect to time, using the fact that dS/dt equals the carbon allocated for wood growth (G_W), gives the diameter growth equation:

$$\frac{dD}{dt} = \frac{G_W}{0.25\pi\Lambda\rho_w\alpha_z(2+\theta_z)D^{1+\theta_z}} \quad (7)$$

This equation transforms the carbon gain from photosynthesis to the diameter growth that results from wood allocation and allometry (Eq 5). With an updated tree diameter, we can calculate the new tree height and crown area using allometry equations, and the targets of leaf and fine root biomass (Eq. 5). Generally, the growing-season average allocations of carbon and nitrogen to different tissues are governed by two parameters: the maximum leaf area per unit crown area (l_{\max}) and fine root area per unit leaf area (ϕ_{RL}) (Eq. 5). The optimal-growth allocation scheme combined with explicit competition for light and soil resources in our model makes it possible to simulate the underlying processes that determine emergent allocation patterns (Weng et al., 2019; Farrior et al., 2013; Dybzinski et al., 2011; Farrior, 2019).

Reproduction and Mortality

At a yearly time-step, the cumulative carbon and nitrogen allocated for reproduction by a canopy cohort over the growing season length, T , is converted to seedlings according to the initial plant biomass (S_0) and germination and establishment probabilities (p_g and p_e , respectively).

Generally, the population dynamics can be described by a variant of the von Foerster equation (von Foerster, 1959):

$$N(S_0, t) = \frac{p_g p_e}{S_0} \int_0^T N(\tau) G_F(\tau) d\tau$$

$$\frac{dN(s, t)}{dt} = -\mu(s, t) N(s, t). \quad (8)$$

Deleted: Wood tissue growth (G_W) drives the growth of tree structure, such as diameter, height, and crown area, and thus increases the targets of leaves and fine roots. By differentiating the stem biomass allometry in Eq. 5 with respect to time, using the fact that dS/dt equals the carbon allocated for wood growth (G_W), we have the diameter growth equation:

$$\frac{dD}{dt} = \frac{G_W}{0.25\pi\Lambda\rho_w\alpha_z(2+\theta_z)D^{1+\theta_z}}$$

... [2]

435 where $N(S_0, t)$ is the spatial density of newly generated seedlings, $N(\tau)$ is the spatial density of
 436 this cohort of trees at time τ , G_F is the carbon allocation to seeds, and μ is PFT-specific mortality
 437 parameter

438 Each PFT has a canopy-layer-specific background mortality rate that is assigned from the
 439 literature. These background rates are assumed to be size-independent for the canopy layer trees,
 440 but size-dependent for understory trees. Many factors affect tree mortality, such as light, size,
 441 competition crown damage, hydraulic failure, trunk damage etc. (Zuleta et al., 2022; Lu et al.,
 442 2021). These factors result in high mortality rates of seedlings and old trees (i.e., a “U-shaped”
 443 mortality curve). We use the following equation to delineate a mortality rate that varies with
 444 social status (crown layers), shade effects, and tree sizes;

$$\mu(s, t) = \mu_0(1 + f_L f_s) f_D \quad (9)$$

445 where f_L is the shade effects on mortality ($f_L = \sqrt{L-1}$), f_s is seedling mortality when a tree is
 446 small ($f_s = A_{SD} e^{-B_{SD} \cdot D}$), and f_D represents the size effects on the mortality of adult trees ($f_D =$
 447 $m_s \frac{e^{A_D(D-D_0)}}{1 + e^{A_D(D-D_0)}}$). L is the layer this plant is in ($L=1$ for the canopy layer and 2 for the second,
 448 and so on), A_{SD} is the maximum multiplier of mortality rate for the seedlings in the understory
 449 layers, B_{SD} is the rate of mortality decreasing as tree diameter (D) increases, m_s is the maximum
 450 multiplier of mortality rate for large-sized trees, D_0 is the diameter at which the mortality rate
 451 increases by $m_s/2$, and A_D is a shape parameter (i.e., the sensitivity to tree diameter).

452 Crown self-organization and layering

453 Tree crowns are arranged into different vertical canopy layers according to tree height and
 454 crown area if their total crown area is greater than the land area following the rules of the PPA
 455 model (Strigul et al., 2008). In PPA, individual tree height is defined as the height at the top of

Deleted:

Formatted: Indent: First line: 0.38"

Deleted: ¶

Deleted: Where

Deleted:

Formatted: Font: Italic

Formatted: Subscript

Deleted:

Deleted:

Deleted:

the crown, and all leaves of a given cohort are assumed to belong to a single canopy layer. The height of canopy closure for the top layer is referred to as critical height (Z^* , the height of the shortest tree in the layer) and is defined implicitly by the following equation:

$$k(1 - \eta) = \sum_i \int_{Z^*}^{\infty} N_i(Z, t) A_{CR,i}(Z^*, Z) dZ \quad (10)$$

where $N_i(Z, t)$ is the density of PFT i trees of height Z per unit ground area; $A_{CR,i}(Z^*, Z)$ is the crown area of an individual PFT i tree of height Z ; η is the proportion of each canopy layer that remains open on average due to wind and imperfect spacing between individual tree crowns, and k is the ground area. The top layer includes the tallest cohorts of trees whose collective crown area sums to $1 - \eta$ times the ground area; lower layers are similarly defined.

All the trees taller than the critical height can get full sunlight and all trees below this height are shaded by the upper layer trees. Trees within the same layer do not shade each other, but there is self-shading among the leaves within individual crowns. Cohorts in a sub-canopy layer are shaded by the leaves of all taller canopy layers. In each canopy layer, all cohorts are assumed to have the same incident radiation on the top of their crowns. Note, the gap fraction η is necessary to allow additional light penetration through each canopy layer for the persistence of understory trees in monoculture forests in which the upper layer crowns build a physiologically-optimal number of leaf layers (Farrior et al., 2013). The grasses only form one layer. Those individuals who cannot stay in that layer because of limited space will be killed (i.e., when the total grass crown area is larger than the land area).

Ecosystem carbon and nitrogen biogeochemical cycles

Ecosystem biogeochemical cycles (carbon and nitrogen in this model) are driven by plant and microbial demographic processes. There are seven pools in each plant: leaves, fine roots,

Deleted: With the PPA model, a key parameter for light competition, the height of canopy closure (i.e., critical height, H^*), is defined; all the plants above this context-dependent height get full sunlight and all trees below this height are shaded by the upper layer trees.

Deleted: ¶

Deleted:

Deleted:

496 sapwood, heartwood, fecundity (seeds), and non-structural carbohydrates and nitrogen (NSC and
 497 NSN, respectively). The carbon and nitrogen in plant pools enter soil pools with the mortality of
 498 individual trees and the turnover of leaves and fine roots. Soil has a mineral nitrogen pool for
 499 mineralized nitrogen and five soil organic matter (SOM) pools for carbon and nitrogen:
 500 metabolic litter (x_1), structural litter (x_2), microbial (x_3), and fast (x_4) and slow-turnover (x_5) SOM
 501 pools.

502 The microbial pool plays a central role in the transfer and decomposition of SOM. The
 503 decomposition processes are simulated by a model modified from Manzoni et al. (2010). The
 504 technical details have been described in detail in Weng et al. (2019, 2017). The decomposition
 505 rate of a SOM pool is determined by the basal turnover rate together with soil temperature and
 506 moisture following the formulation of the CENTURY model. The microbial carbon use
 507 efficiency (transfer from litter to microbial matter) is a function of litter nitrogen content,
 508 following the model of Mazoni et al. (2010).

509 The N mineralization in decomposition is determined by microbial nitrogen demand,
 510 SOM's C:N ratio, and decomposition rate. In the high C:N ratio SOM, microbes must consume
 511 excess carbon to get enough nitrogen for growth. By contrast, in the low C:N ratio SOM,
 512 microbes must release excess nitrogen to get enough carbon for energy. Depending on the C:N
 513 ratios of SOM, soil microbes may be limited by either C or N.

514 The out-fluxes of C and N from the i^{th} pool (dC_i and dN_i , respectively) are calculated by:

$$\begin{aligned} dC_i &= \xi(T, M) \rho_i Q C_i, \\ dN_i &= \xi(T, M) \rho_i Q N_i, \end{aligned} \tag{11}$$

515 where ζ is the response function of decomposition to soil temperature (T) and moisture (M), ρ_i is
 516 the basal turnover rate of the i^{th} litter pool at reference temperature and moisture, QC_i is the C
 517 content in i^{th} pool, and QN_i is the N content in the i^{th} pool.

518 The new microbial growth (dM) is calculated as the co-limit of available carbon and
 519 nitrogen mobilized at this step:

$$dM_i = \text{Min}(\varepsilon_0 \cdot dC_i, A_{\text{microbe}} \cdot dN_i), \quad (12)$$

520 where ε_0 is default carbon-use efficiency of litter decomposition (0.4) and A_{microbe} is a microbe's
 521 C:N ratio, which is a fixed value (10 in this model). The soil heterotrophic respiration (R_h) is the
 522 microbial respiration (i.e., the difference between carbon consumption and new microbial
 523 growth), and the total N mineralization rate ($N_{\text{mineralized}}$) is calculated as the sum of mineralized N
 524 in the SOM pools and microbial turnover:

$$R_h = \sum_{i=3}^5 dC_i - \sum_{i=4}^5 M_i, \quad (13)$$

$$N_{\text{mineralized}} = \sum_{i=3}^5 dN_i - \sum_{i=3}^5 m_i / A_{\text{microbe}}$$

525 The R_h releases to atmosphere as CO_2 . Mineralized N enters the mineral N pool for plants to use.

526 The dynamics of the mineral N pool is represented by the following equation:

$$\frac{dN_{\text{mineral}}}{dt} = N_{\text{deposition}} + N_{\text{mineralized}} - U - N_{\text{loss}}, \quad (14)$$

527 where $N_{\text{deposition}}$ is N deposition rate, assumed to be constant over the period of simulation; N_m is
 528 the N mineralization rate of the litter pools (fast and slow SOM and microbes); U is the N uptake
 529 rate ($\text{Kg N m}^{-2} \text{ hour}^{-1}$) of plant roots; and N_{loss} includes the loss of mineralized N by
 530 denitrification and runoff. The N deposition ($N_{\text{deposition}}$) is the only N input to ecosystems, and we
 531 set nitrogen fixation as zero in this version of the model.

532

Formatted: Subscript

533 3 Model Test runs

534 For our comparison of model performance against observations and other models, we used
535 the full demographic version of BiomeE (described above) and also designed a “single-cohort”
536 version of the model to benchmark our demographic implementations. In the single-cohort
537 model, the mortality of trees is simulated as the turnover of woody biomass, and the fecundity
538 resources (carbon and nitrogen) are used to build the same-sized parent trees, instead of
539 seedlings growing from understory layers. If the total crown area of the trees in this cohort is
540 greater than the land area, the extra trees will be removed to make the total crown area less than
541 or equal to the land area. At equilibrium, the turnover of woody biomass is equal to the new
542 growth each year and the new trees generated from fecundity resources are killed by self-
543 thinning. The single-cohort model uses the mean state of the canopy layer trees to represent the
544 characteristics of the whole community. This single-cohort model performs like the traditional
545 biogeochemical models and simplifies vegetation computation.

546 In the test runs, the distribution of PFTs was from the Ent vegetation map (Ito et al., 2020),
547 which is derived from 2004 MODIS land cover and PFT data products (Friedl et al., 2010) and
548 climate data (Fig. 2). For these simulations, croplands and pastures were replaced by the
549 potential natural vegetation types.

550

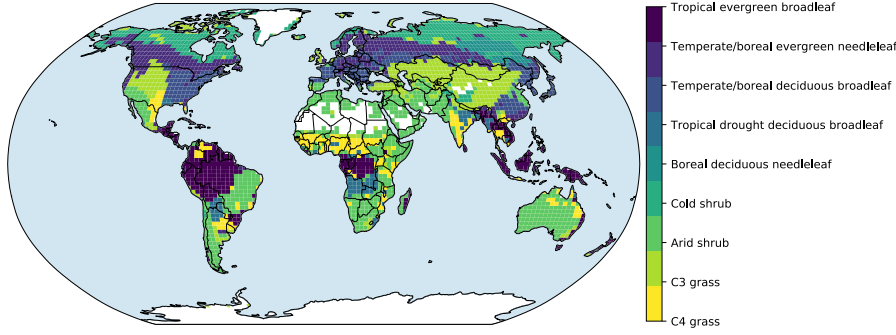


Figure 2. Prescribed global distribution of plant functional types. Data is from the Ent Global Vegetation Structure map.

Forcing data are from the TRENDY project CRU-NCEP data (Sitch et al., 2015) and have a 6-hour time step at a spatial resolution of $0.5^\circ \times 0.5^\circ$. These data are available at the website <https://www.uea.ac.uk/web/groups-and-centres/climatic-research-unit/data>.

We aggregated these data into $2.0^\circ \times 2.5^\circ$ grid cells and used thirty years' of data (1988–2017) to force the model to run for 600 years, which is long enough for the model to approach equilibrium states for both vegetation and soil carbon pools. These data include temperature, precipitation, shortwave radiation, longwave radiation, specific humidity, and wind speed (U and V directions). We interpolated the radiation data (R_s) into half-hour timesteps based on the sun zenith angle (θ_s) and radiation penetration rate calculated from data.

$$R_s(t) = \left(\frac{R_{H6}}{S^* \cos \theta_s(H6)} \right) S^* \cos \theta_s(t), \quad (15)$$

where S^* is solar constant (1362 W/m^2). Other variables are linearly interpolated to the model time steps, which is half hourly in this study. CO_2 concentration is set at the model default level (350 ppm) in our model runs.

Formatted: Font: Italic

Formatted: Subscript

Formatted: Font: Italic

Formatted: Subscript

567 **Data sources for model evaluation**

568 **Gross primary productivity (GPP) data** are from a global retrieval of surface turbulent fluxes
569 including latent heat, sensible heat, and GPP using remote sensing observations. These data are
570 on a $1^{\circ} \times 1^{\circ}$ geographic grid at a monthly time step based on an Artificial Neural Network
571 retrieval algorithm (Alemohammad et al., 2017). This algorithm uses six remotely sensed
572 observations as input: Solar Induced Fluorescence (SIF), Air Temperature, Precipitation, Net
573 Radiation, Soil Moisture, and Snow Water Equivalent. The data are available from 2007 to 2015.

574 **The tree height data** are from spaceborne light detection and ranging (lidar) global map of
575 canopy height at 1-km spatial resolution developed by Simard et al. (2011). These authors used
576 the 2005 data from the Geoscience Laser Altimeter System (GLAS) aboard ICESat (Ice, Cloud,
577 and land Elevation Satellite) to derive global forest canopy heights. **Biomass data** are from a
578 Global 1-degree Maps of Forest Area, Carbon Stocks, and Biomass, 1950-2010 developed by
579 Hengeveld et al. (2015). **Soil carbon data** are from Food and Agriculture Organization (FAO)
580 Harmonized World Soil Database (version 1.2), updated by Wieder et al. (2014).

581 **MsTMIP model simulation data**

582 We chose six model simulations (BiomeBGC, CTEM, CLM4, LPJ, Orchidee, VEGAS) from the
583 Multi-scale Synthesis and Terrestrial Model Intercomparison Project (MsTMIP) (Huntzinger et
584 al., 2012) to compare against our model simulations. These models are well-developed and
585 widely used in Earth system models, representing the state-of-art of current land vegetation
586 model development. MsTMIP provided prescribed land use types for all the participant models.
587 However, it is up to the participant models for disturbance impacts on ecosystems (Huntzinger et
588 al., 2013). MsTMIP conducted five sets of experimental runs with different climate forcing,
589 land-use history, atmospheric CO₂ concentration, and nitrogen deposition. In this study, we used

Formatted: Subscript

the SG1 simulation experiment because it is driven by the 1901~2010 climate forcing data with constant CO₂ concentration and constant land cover (Huntzinger et al., 2013), which are the closest to our model runs.

Formatted: Subscript

Deleted: (Huntzinger et al., 2013)the because it is driven by the 1901~2010 climate forcing data with constant CO₂ concentration and constant land cover (Huntzinger et al., 2013),which closest

Selected Grid Cells for Comparison

To illustrate model behavior, we selected 8 grid cells that cover boreal forests, temperate forests, tropical forests, C₄ grasslands, and arid shrublands to show the simulated ecosystem development patterns across the climate zones with different dominant PFTs (Table 2). Brazil Tapajos (TPJ), Oak Ridge (OKR), Harvard Forest (HF), Manitoba old black spruce site (MNT), and Bonanza Creek (BNC) are covered by tree PFTs. Konza long-term ecological research station (LTER) (KZ) is C₄ grass. Walnut Gulch Kendall (WKG) and Sevilleta LTER (SV) are covered by arid shrubs. These sites were chosen because they have extensive data on vegetation and climate conditions for future comparisons.

Formatted: Indent: First line: 0.38", Line spacing: Double

Deleted: ¶

Table 2 Sites for simulated ecosystem development illustration

Site	Dominant PFT	Coordination	Mean Temperature (°C)	Annual Precipitation (mm)
Bonanza Creek (BNC)	Broadleaf deciduous	63.92°, -145.38°	-3.1	269
Manitoba old black spruce site (MNT)	Evergreen needleleaf	55.88°, -98.48°	-3.2	520
Harvard Forest (HF)	Broadleaf deciduous	42.54°, -72.17°	8.5	1050
Oak Ridge (OKR)	Broadleaf deciduous	35.96°, -84.29°	13.7	1372
Konza LTER (KZ)	C ₄ grass	39.08°, -96.56°	12.4	835
Sevilleta LTER (SV)	Arid shrub	34.36°, -106.88°	12.7	365
Walnut Gulch Kendall (WKG)	Arid shrub	31.74°, -109.94°	17.7	350
Brazil Tapajos (TPJ)	Broadleaf evergreen	-2.86°, -54.96°	26	1820

Deleted: ¶

4 Results

4.1 Simulated vegetation structural and ecosystem carbon dynamics

In the forest sites, the simulated vegetation structure by the full demographic model changes with the growth, regeneration, and mortality processes (Fig. 3). It can be separated into three stages according to the canopy crown dynamics: 1) open forest stage, 2) self-thinning stage, and 3) stabilizing stage. In the open forest stage, the crown area index (CAI) is less than 1.0 and all the individuals are in full sunlight. The tree crowns grow rapidly to occupy the open space (Fig. 3: a). In the self-thinning stage, the open space is filled by the crowns of similar sized trees (i.e., the forest is closed) and canopy trees are continuously pushed to the lower layer(s) (i.e., self-thinning) and the CAI continues to increase due to the limited space with growing tree crowns (i.e., the new spaces vacated from the canopy trees' mortality cannot meet the space demand from crown growth). The sizes of trees in the canopy layer are still similar in this period (Fig. 3: b and c) and the critical height (the height of the shortest tree in the canopy layer) keeps increasing in this period. In the stabilizing stage, when the space generated by the mortality of canopy trees is larger than the growth of canopy tree crown area, no trees are pushed to the lower layer and the lower layer trees start to enter the canopy layer and fill the space, leading to a sharp decrease in critical height (Fig. 3: b) and the mixing of different sized trees in the canopy layer. The CAI is decreasing as well because of the high mortality rates of the understory layer trees. As time goes on, the growth, regeneration, mortality, and space filling processes are equilibrated, and the forest structure is then stabilized.

The tallest plant height (Fig. 3: c) shows the height of the trees in the tallest cohort. It keeps growing as this cohort exists. The sharp decreases indicate the replacements by or merging with another shorter cohort because the density of trees in this cohort is very low (0.0001/ha in this

Deleted: 4.1 Simulated ecosystem dynamics in different climate zones

Formatted: Font: Bold

Formatted: Font: Bold

Formatted: Indent: First line: 0.38"

case) or the similarity between the tallest and the second tallest is high. The total basal area (Fig. 3: d) is an index of the sum of all trees at a site. It keeps increasing during forest development and is equilibrated earlier than height and crown structure.

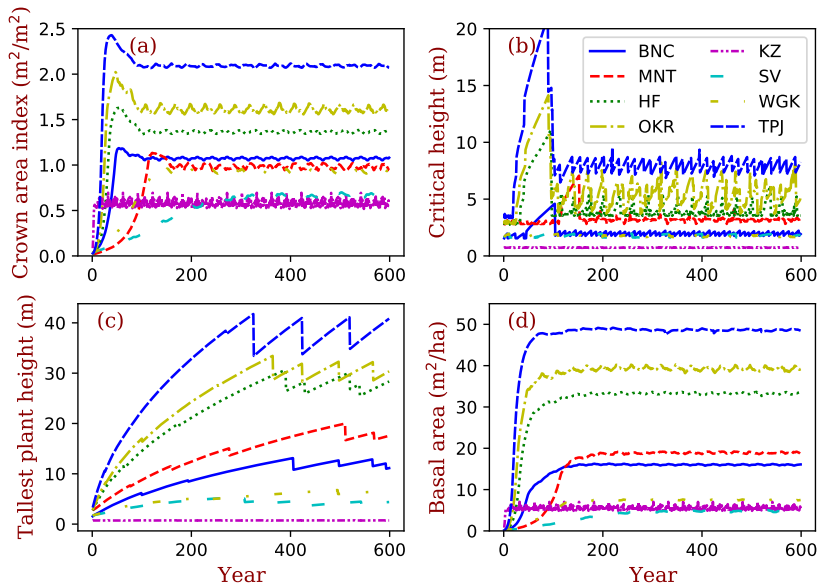
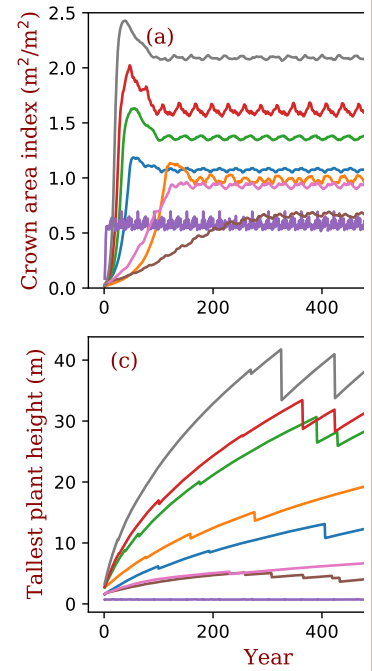


Figure 3. Vegetation structural dynamics with full demography functions. Critical height is an emergent property of the model PPA, which separates the trees that are in full sunlight if taller than critical height and those that are fully shaded if shorter than critical height.

Among these sites, at equilibrium, the tropical forest site (TPJ) has the highest crown area index (around 2.2), followed by warm temperate forest at OKR, mixed forest at HF, and boreal forests at BNC and MNT (Fig. 3). The shrubs and grasslands in arid regions have the lowest crown area index (CAI), with basal area following similar patterns. For forested sites, tree height is tallest at

Deleted: structure by model changes with the growth, regeneration, and mortality processes (Fig. 3). It according to the canopy crown dynamics be the Compared to the CAI (Fig. 3: a) and critical height (Fig. 3: b), The tallest plant height (Fig. 3: c) shows the height of the trees in the tallest cohort. It keeps growing as this cohort exists. The sharp decreases indicate the replacements by or merging with another shorter cohort because the density of trees in this cohort is very low (0.0001/ha in this case) or the similarity between the tallest and the second tallest is high. The total basal area (Fig. 3: d) is an index of the sum of all trees at a site. It keeps increasing during forest development and is equilibrated earlier than height and crown structure.



Deleted:

TPJ, followed by OKR, HF, MNT, and BNC. The shrubs are short according to their allometry parameters and the height of grasses during non-growing season is zero. The critical height, which separates canopy layer trees from the understory layers, follows the same order as that of tree height with high fluctuations with cohort changes.

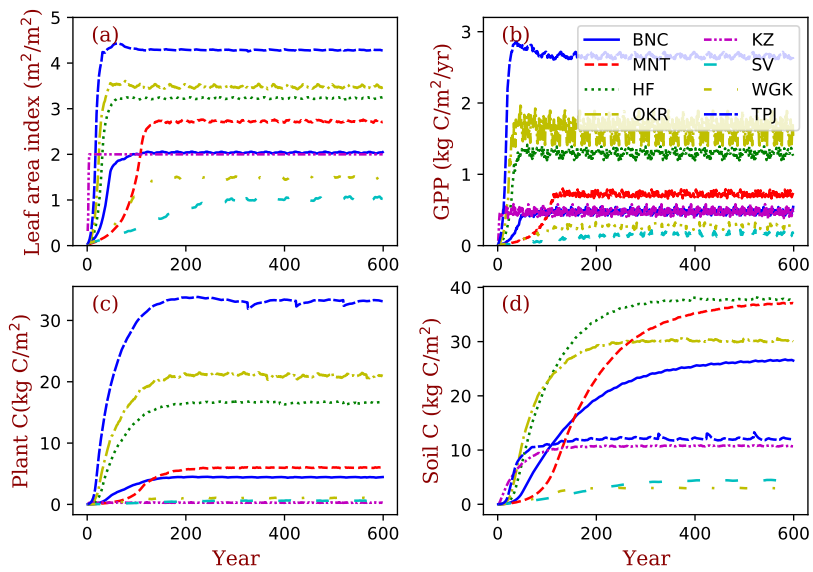


Figure 4: Site ecosystem development simulated by BiomeE with full demography.

For the temporal dynamics in the full demographic simulations (Fig. 4), the simulated GPP aligns closely with LAI and they reach their equilibrium states at similar times across sites (Fig. 4: a,b). According to the definition of maximum crown LAI (I_{max}) in Eq. 6, the grass LAI (i.e., Konza) reaches the maximum each year, except the first year due to the low initial density (Fig. 4: a). The biomass accumulation is much slower in forests because of the longer time needed for forest structure (size distribution) to reach equilibrium. Soil carbon equilibration is faster in the

Formatted: Centered

Deleted: ¶
Among these sites, at equilibrium, (The tropical forest site (TPJ) has the highest crown area index (around 2.2), followed by warm temperate forest at OKR, mixed forest at HF, and boreal forests at BNC and MNT (Fig. 4). The shrubs and grasslands in arid regions have the lowest crown area index (CAI), with basal area following similar patterns. For forested sites, tree height is tallest at TPJ, followed by OKR, HF, MNT, and BNC. The shrubs are short according to their allometry parameters and the height of grasses during non-growing season is zero. The critical height, which separates canopy layer trees from the understory layers, follows the same order as that of tree height with high fluctuations with cohort changes.

Formatted: Font: Bold

Deleted:

Formatted: Centered, Indent: First line: 0", Line spacing: Multiple 1.15 li

Deleted: Equilibrium time scales for

Deleted: reach their equilibrium states at similar times across sites, but biomass accumulation is much slower in forests because of the longer time needed for forest structure (size distribution) to reach to approach equilibrium. Soil carbon equilibration is faster in the warm regions than in cold regions because of the higher turnover rate of SOM pools in warm regions.

Formatted: Font: Italic

Formatted: Subscript

warm regions than in cold regions overall because of the higher turnover rate of SOM pools in warm regions. At equilibrium, forested sites have higher LAI, biomass, and carbon stocks per area compared to the shrub and grass sites overall. Vegetation biomass is lowest at the grassland site (i.e., Konza) because, within the model, grassland ecosystems cannot accumulate persistent woody biomass.

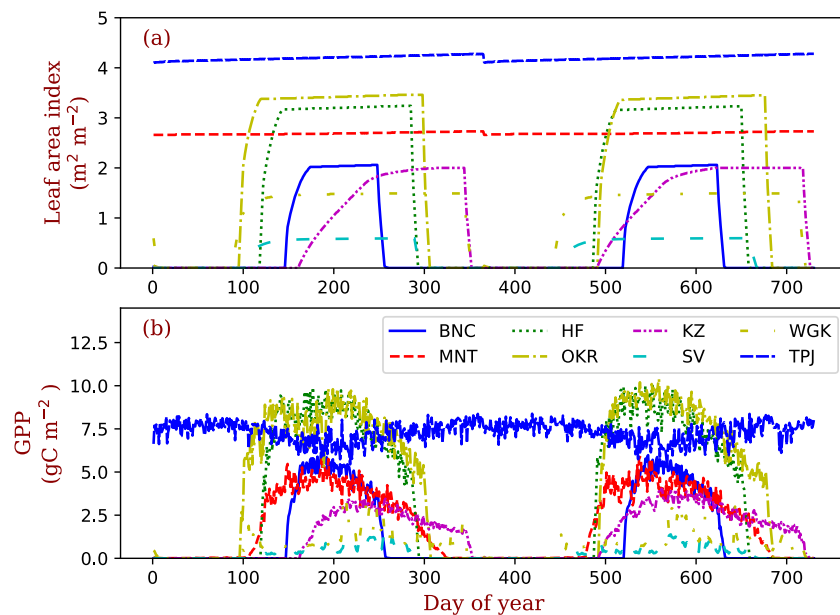
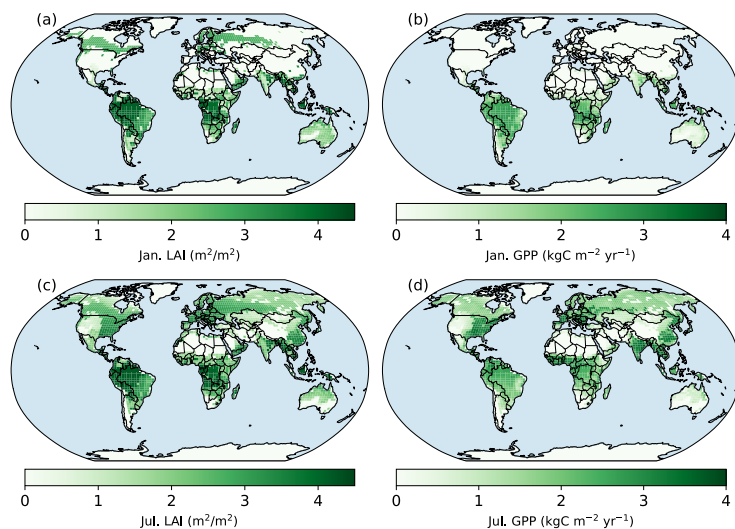


Figure 5. Seasonal patterns of LAI and gross primary production in the sample grids. Two years of data are shown in this figure. The key of location abbreviations is in Table 2.

The PFTs at TPJ and MNT are evergreen ~~trees~~. Their LAI does not change over the whole year (Fig. 5: a). The forest in OKR has the longest growing season in the three deciduous forest grids, followed by HF and BNC. BNC's growing season is only around 120 days, about half of OKR's growing season. The growing season of grasses in KZ starts in late May and ends in

Deleted: trees forest.

712 September. The two arid-adapted shrub sites (SV and WKG) are controlled by water availability.
 713 In TPJ (tropical evergreen forest), the trees have photosynthesis throughout the entire year (Fig.
 714 5: b). In MNT, photosynthesis only happens in warm seasons with the leaves kept in the crowns
 715 (evergreen needleleaf). The deciduous trees in OKR and HF have high photosynthesis rates
 716 during the growing season. The photosynthesis rates in SV and WKG are generally low because
 717 of the relatively dry environment. However, the precipitation events can drive photosynthesis
 718 rates high in these arid regions. At the global spatial scale, only evergreen needle-leaved forests
 719 keep their leaves in northern high latitude regions during January (Fig. 6), though photosynthesis
 720 in this region ceases because of the low temperature. In July, northern high latitude regions green
 721 up and their photosynthesis rates are high in wet regions.



722
 723 **Figure 6. Spatial patterns of LAI and GPP in Jan and July simulated with full**
 724 **demographic BiomeE.** Panels a and b are the LAI and photosynthesis of January in the year of
 725 600 (the last year of model run). Panels c and d are July's in the same year.

Deleted: ¶

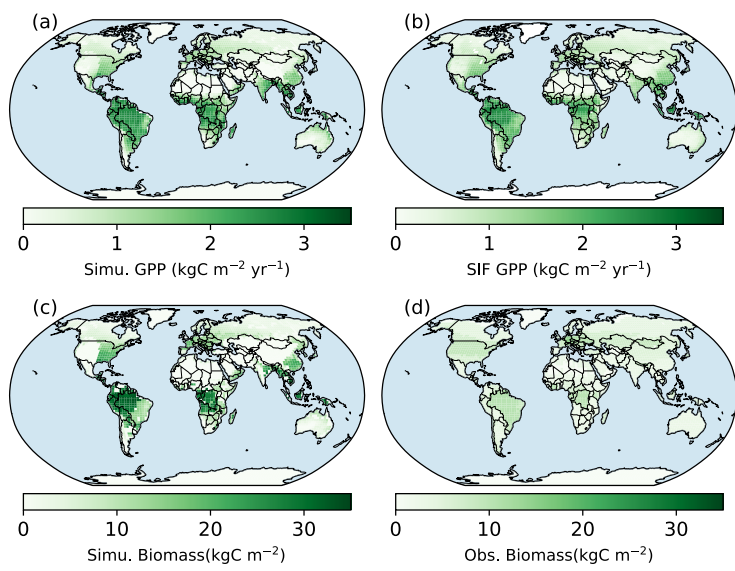
728 **4.2 Global Comparisons with Observations**

729 We tuned the parameter of maximum carboxylation rate (V_{cmax}) to fit the general pattern of
730 global GPP. Compared with SIF GPP (Alemohammad et al., 2017), simulated GPP is higher than
731 the SIF GPP generally (Figs. 7 and 8), though lower in arid regions (Fig. 7). The simulated tree
732 height is mostly taller compared to observations (Simard et al., 2011) because most forests have
733 been altered by human activities (Pan et al., 2013). However, the model and observations cover
734 approximately the same range of tree heights (up to 40 m). Simulated biomass is much higher
735 than the observations because, in the observations, many forest regions have been transformed
736 to low biomass land use types (such as croplands) or represent earlier successional stages with
737 less accumulated carbon (i.e., not equilibrium states).

Formatted: Indent: First line: 0.38", Line spacing: Double

Deleted: most

Deleted:



738

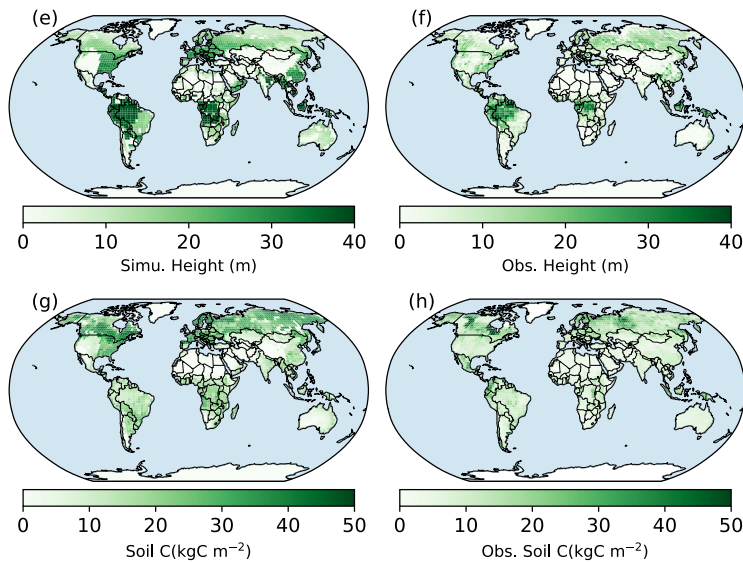


Figure 7. Spatial patterns of BiomeE (full demography) simulations and those from data.

“Obs.” means different way retrieved from observations. Some are model-based (e.g., GPP is from SIF data and tree height is from LiDAR data). Obs. **GPP** is derived from Solar Induced Fluorescence (SIF) data with a machine learning approach (Alemohammad et al., 2017). The data are available from Jan. 2007 to Dec. 2015. **The tree height data** are from spaceborne light detection and ranging (lidar) global map of canopy height at 1-km spatial resolution developed by Simard et al. (2011). **Biomass data** are from Hengeveld et al. (2015). **Soil carbon data** are from FAO Harmonized World Soil Database (version 1.2), updated by Wieder et al. (2014).

Simulated soil carbon does track the observations better than biomass, likely because soil carbon stocks are more stable compared to biomass; and GPP does not change much compared to the changes in vegetation biomass because leaves can reach to equilibrium much faster than the biomass does (Fu et al., 2017). For areas where the model underpredicts soil carbon, the difference could arise from the missing biogeochemical processes that may lead to high carbon accumulation in some regions (e.g., peats) (Davidson and Janssens, 2006; Briones et al., 2014;

Formatted: Indent: First line: 0"

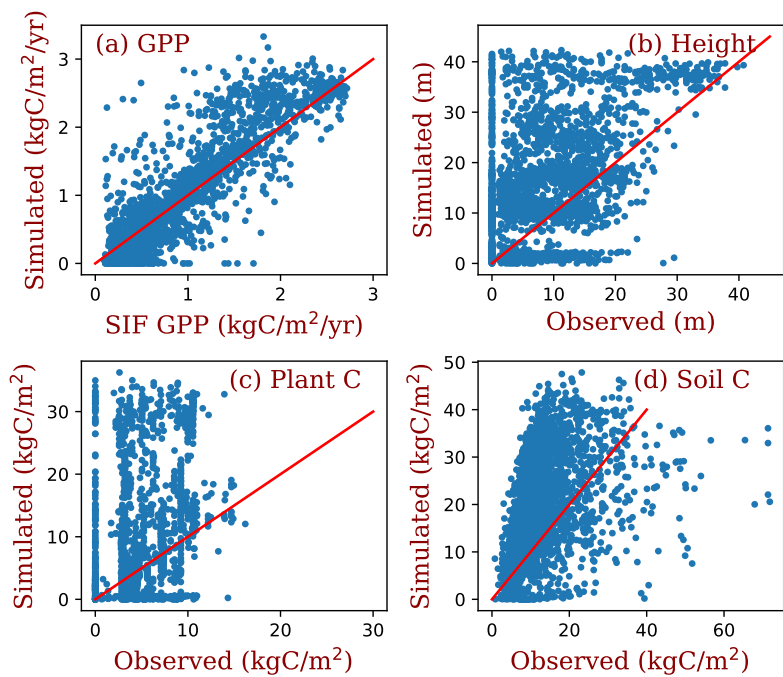
Deleted:

Deleted:

Deleted:

760 Euskirchen et al., 2014), or the relatively high uncertainties in the soil carbon data (Tifafi et al.,
 761 2018).

762



763

764 **Figure 8. Grid comparison of full demographic BiomeE simulations with observations**
 765 **estimates.** The red line in each panel is the 1:1 line. This figure uses the same simulated and
 766 observed data as those of Figure 7.

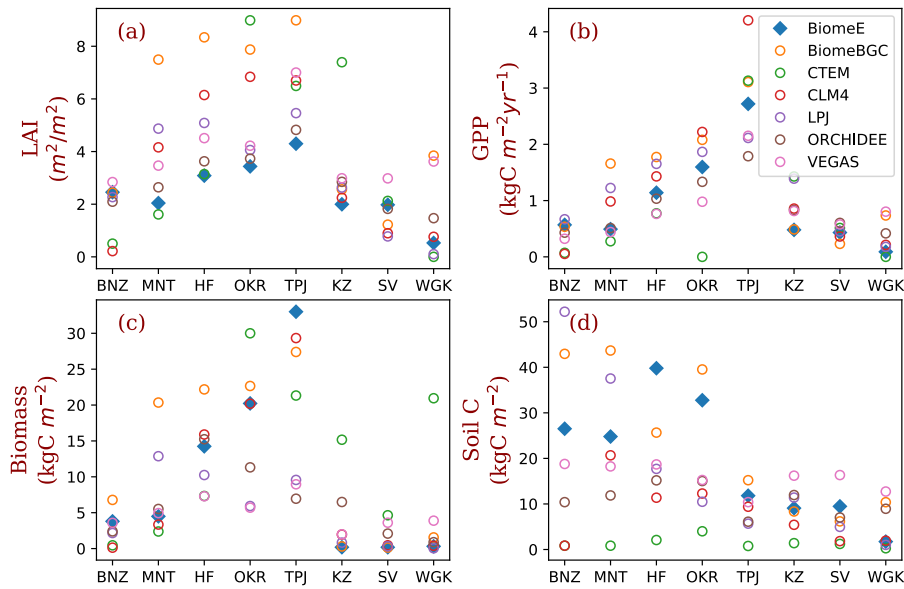
767

768 **4.3 Comparison with MsTMIP models**

769 We compared the performance of our model with MsTMIP models at the 8 locations that
 770 were used to show ecosystem development patterns (Table 2). For most of these sites, LAI in
 771 BiomeE is lower compared the other MsTMIP models (Fig. 9: a), while the estimated GPP is

775 within the range of MsTMIP predictions (Fig. 9: b). LAI differences are a consequence of the
 776 formulations within BiomeE. Specifically, BiomeE simulates leaf growth by using a maximum
 777 crown LAI, which is lower than the real forest LAI. However, the low LAI does not affect crown
 778 total photosynthesis because leaves in lower canopy layers contribute little to the total carbon
 779 assimilation. BiomeE predicted biomass (Fig. 9: c) and soil carbon (Fig. 9: d) generally fall
 780 towards the higher end of the MsTMIP simulations, except for the more arid grass- and shrub-
 781 dominated sites. We note, however, that there are wide differences in estimates for vegetation
 782 and soil carbon across the models, likely because of different treatments of mortality and
 783 decomposition functions in these models.

784

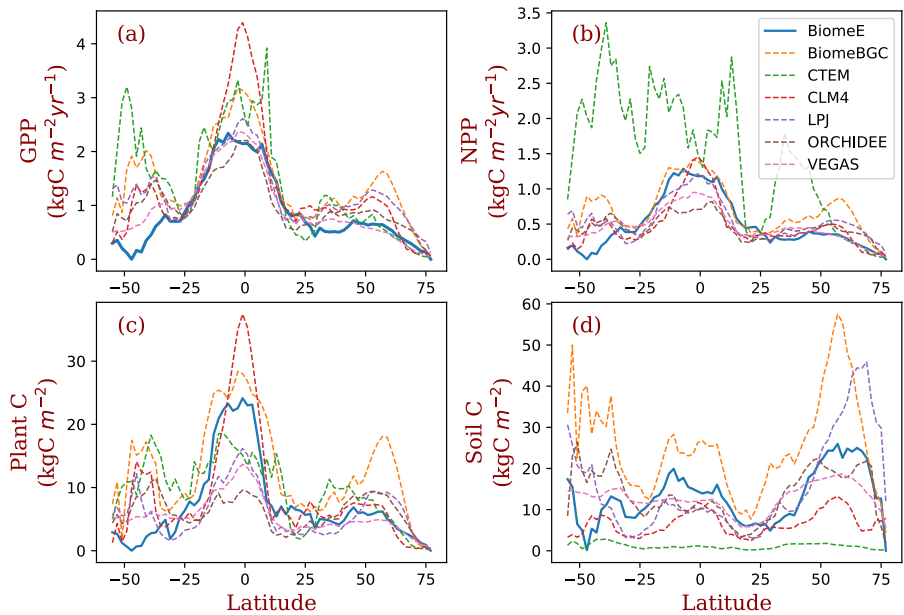


785

786

Figure 9 Site-level comparison with MsTMIP models.

787 The BiomeE predictions are from the full demography. The abbreviations of the 8 sites
 788 (corresponding to model grid cells) and their coordination, dominant PFTs, and climatic
 789 conditions are in Table 2.
 790



791
 792 **Figure 10 Latitudinal patterns of GPP, NPP, Biomass, and soil carbon as simulated by**
 793 **BiomeE (with full demography) and MsTMIP models**

794
 795 More broadly, the latitudinal mean of BiomeE simulated GPP is at the lower end of MsTMIP
 796 model predictions (Fig. 10: a). Since BiomeE's GPP was tuned to fit remote sensing data derived
 797 GPP, the MsTMIP models may over-estimate global GPP. BiomeE simulated NPP (Fig. 10: b),
 798 plant carbon (Fig. 10: c), and soil carbon (Fig. 10: d) are within the range simulated by the
 799 MsTMIP models. This indicates that BiomeE has slightly lower respiration than the MsTMIP
 800 models. In the arid regions (e.g., around latitude 40-50°S), our model's GPP is lower than
 801 MsTMIP's because of sensitive drought responses in our model.

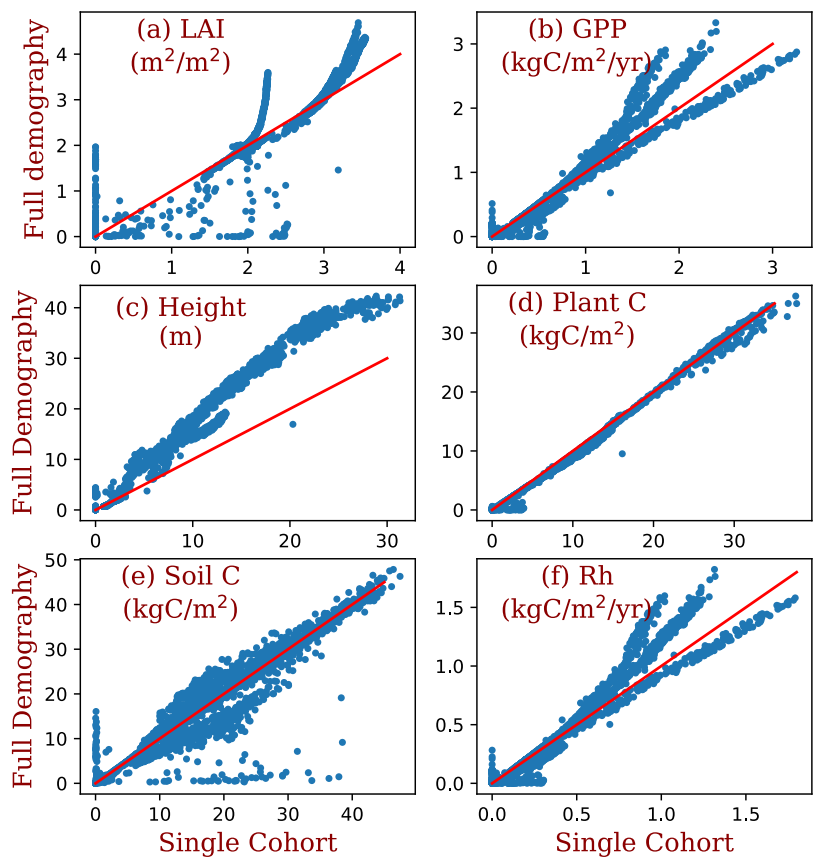


Figure 11 Comparison between the simulations of the full demography and the single cohort settings of BiomeE.

The demographic processes have significant impacts on the simulations of GPP, biomass, soil carbon, and vegetation structure compared to the single-cohort version of BiomeE (Fig. 11). The demographic version of the model includes an understory layer of plants, resulting in higher LAI in high LAI regions and also slightly higher GPP. Higher GPP in the model with full

811 demography leads to a high allocation to leaves and fine roots. However, the total biomass
812 predicted by the two model versions are similar because of the tradeoffs in allocation between
813 leaves and stem growth and tree size distribution and because most biomass is concentrated in
814 stems. In the full demography model, tree mortality removes all the biomass, including leaves,
815 fine roots, and stems, while in the single-cohort model, the mortality is represented as the
816 turnover of woody biomass. Consequently, the full demography model has higher emergent
817 turnover rate for the whole vegetation.

818 Compared to the single-cohort model, the full demography model predicts higher LAI and
819 GPP in warm and wet regions and lower values in cold and dry regions (Fig. 12: a, b). The full
820 demography model also predicts much lower biomass and soil carbon than the single-cohort
821 model in cold and dry regions (Fig. 12: c). Because the single cohort model has the same SOM
822 pools and turnover/decomposition processes, the reduced biomass input from full demography
823 alone is causing the difference in SOM dynamics. This is consistent with the functions of
824 demographic processes in these regions, which greatly reduce model stability because
825 reproduction and survival are lower in dry and cold regions. By contrast, the single-cohort model
826 does not model these processes explicitly and instead uses a simplified routine turnover of
827 materials that allows plants to stay in extremely dry or cold conditions.

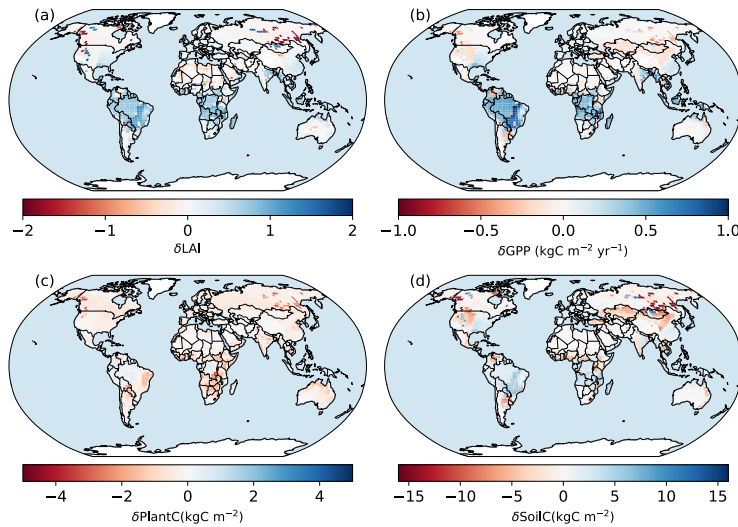


Figure 12. Spatial patterns of the differences between the simulations of the BiomeE: full demography minus the single-cohort versions.

4.4 Eco-evolutionary simulation and sensitivity test

This model has the potential to predict competitively dominant PFTs in the continuum of plant traits through succession simulations according to the principles of evolutionarily optimal competition strategy. We illustrate this with a set of simulations conducted at a series of ecosystem nitrogen content (from 269 to 575 g N/m^2) with five PFTs sampled from the continuums of LMA (σ , from 0.06 to 0.14) and target root/leaf area ratio (ϕ_{RL} , from 0.8 to 1.2 corresponding to each LMA). The different ecosystem total nitrogen represents the environmental conditions that can result from soil and climate conditions. The simulations are set as nitrogen-closed (i.e., no input and output of nitrogen). At the lowest ecosystem total nitrogen (Fig. 13: a), the PFT with highest LMA (0.14 kg C/m^2 leaf) wins. With increases in ecosystem nitrogen (Fig. 13: b~d), the winner shifts to lower LMA PFTs. This means that in infertile soils

Deleted:

Deleted:

Formatted: Font: Bold

Formatted: Line spacing: Double

Formatted: Left, Line spacing: Double

Formatted: Superscript

Formatted: Font: Italic

or cold climates with slower biogeochemical cycles (e.g., tundra and boreal forests), the evolutionarily optimal PFTs should have high LMA leaves, and vice versa. This pattern is consistent with the predictions of a theoretical model derived in Weng et al. (2017). This simulation is also a case of sensitivity of simulated vegetation dynamics to environmental conditions. Vegetation can shift their compositions and dominant plant traits to maintain an evolutionarily optimal state, and thus amplify or attenuate the responses of ecosystem carbon cycle to climate changes.

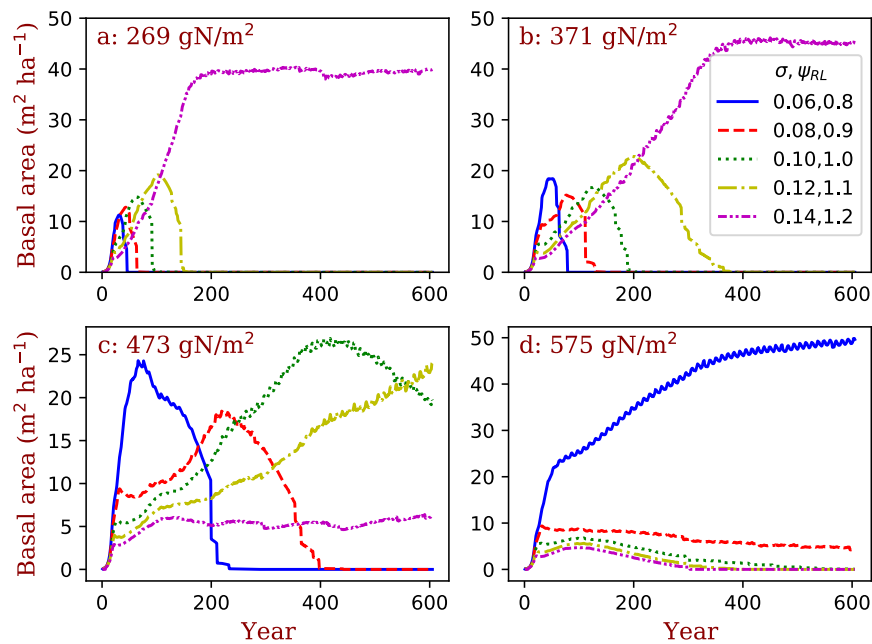


Figure 13. Simulated competitively dominant PFTs at different total ecosystem nitrogen. The simulations are set as nitrogen-closed (i.e., no input and output of nitrogen). The number in the title of each panel is the initial soil nitrogen. We used five PFTs that only differed in their LMA (σ) and target root/leaf area ratio (ψ_{RL}) corresponding to each LMA in each simulation.

Deleted: ¶

861

862 5 Discussion

863 We developed a parsimonious terrestrial ecosystem model for ModelE to simulate vegetation
864 dynamics and biogeochemical cycles. This model includes a cohort-based representation of
865 vegetation structure, a height structured light competition scheme, demographic processes, and
866 coupled carbon-nitrogen biogeochemical cycles. This model has four major modules that
867 organize the hierarchical processes of ecosystems together into a cohesive modeling structure: 1)
868 plant physiology (photosynthesis, respiration), 2) plant phenology and growth, 3) vegetation
869 structural dynamics, and 4) soil biogeochemical cycles (Fig. 1). Each module is cohesive and has
870 a minimum set of variables as the input from other modules.

871

872 5.1 Model formulation

873 In designing this model, we considered the simulation of competitively optimal strategy of plants
874 in different climates based on fundamental ecological rules (Purves and Pacala, 2008; Falster and
875 Westoby, 2003; Franklin et al., 2020). These strategies are mainly related to light competition,
876 water conditions, nutrient use efficiency, and disturbances (e.g., fire), and represented by the
877 traits of wood density, height growth, leaf longevity, and photosynthesis pathways. PFTs are
878 used in this model as an integrative unit representing combinations of plant traits for simulating
879 (1) the spontaneous dynamics of carbon, water, and energy fluxes as the core functions of an
880 ESM-based land model and (2) the transient vegetation structural and compositional dynamics
881 and ecosystem biogeochemical cycles in response to climate variations.

Formatted: Line spacing: 1.5 lines

Deleted: BiomeE,

Deleted: ,

Moved down [1]: In designing this model, we considered the simulation of competitively optimal strategy of plants in different climates based on fundamental ecological rules (Purves and Pacala, 2008; Falster and Westoby, 2003; Franklin et al., 2020). These strategies are mainly related to light competition, water conditions, nutrient use efficiency, and disturbances (e.g., fire), and represented by the traits of wood density, height growth, leaf longevity, and photosynthesis pathways. PFTs are used in this model as an integrative unit representing combinations of plant traits for simulating (1) the spontaneous dynamics of carbon, water, and energy fluxes as the core functions of an ESM-based land model and (2) the transient vegetation structural and compositional dynamics and ecosystem biogeochemical cycles in response to climate variations.

Moved (insertion) [1]

Deleted:

Formatted: Indent: First line: 0"

900 We adopted a generic design for the PFTs in the standalone BiomeE (Weng et al., 2019):
901 since the PFTs are samples of plant traits in their natural ranges, the numbers of PFTs are
902 flexible, depending on what strategies users wish to test (as the test simulations in Figure 13).
903 This approach substantially simplifies the parameterization of PFTs because it changes the
904 parametrizations to the selections of strategies through choosing different trait values (i.e.,
905 parameters). Thus, the PFTs are adaptive and can change to each other in different climate zones,
906 making it possible to reduce the number of PFTs while representing functional diversity and the
907 optimal adaptation to climate conditions.

908 To represent the major variations in plant functional diversity, we chose four plant traits as
909 the primary axes to define PFTs: wood density, leaf mass per unit area (LMA), height growth
910 parameter, and leaf maximum carboxylation rate (V_{cmax}). Wood density is relatively conservative
911 (Swenson and Enquist, 2007; Chave et al., 2009), mostly ranging from 200 to 500 kg C m⁻³,
912 while herbaceous stem density ranges from 400~600 kg C m⁻³ (Niklas, 1995). However,
913 herbaceous stems are usually hollow, making the ratio of total biomass to its volume low, and
914 grasses shed their stems each growing season, resulting in faster stem turnover. It is a strategic
915 difference from woody plants, which keep the woody tissues to build up their trunks and thus
916 display their leaves on top of trunks for light competition (Dieckmann et al., 2007; Falster and
917 Westoby, 2003). LMA is the key leaf trait that determines leaf life longevity and leaf types (i.e.,
918 evergreen vs. deciduous) (Osnas et al., 2013), and represents the strategy for the competition in
919 different soil nutrient levels (Tilman, 1988; Reich, 2014; Weng et al., 2017) and resistance to
920 stresses of water and temperature (Oliveira et al., 2021).

921 In this model, the phenological type is simulated as an emergent property of plant
922 physiological processes and its strategy to deal with seasonal variations of temperature and water

923 availability. We used three parameters – growing degree days (GDD), running mean daily
924 temperature, and critical soil moisture – to define all possible phenological types. These three
925 parameters are widely used in a variety of phenology models (Sitch et al., 2003; Prentice et al.,
926 1992; Arora and Boer, 2005). As for soil organic matter decomposition, the CASA model is
927 currently used in ModelE; it has 13 pools with different transfer coefficients and turnover rates
928 (Randerson et al., 1997; Potter et al., 1993, 2003). The models developed thereafter have more
929 sophisticated processes, especially those of microbial activities and carbon use efficiency
930 (Manzoni et al., 2010; Wieder et al., 2014; Wang and Goll, 2021). We chose an intermediate
931 complexity scheme that has only two SOM pools but a functional microbial pool for
932 decomposing SOM so that the dynamics of SOM's C/N ratio, carbon use efficiency, and nitrogen
933 mineralization can be reasonably simulated while keeping the model structure parsimonious.

Deleted:

935 **5.2 Model predictions and performance**

936 This model has four relatively distinctive sets of simulated variables that are critical for model
937 performance and calibration: 1) Stomatal conductance, photosynthesis, and respiration; 2)
938 demographic rates (i.e., allocation, structural growth, mortality, and reproduction); 3) LAI, tree
939 size, crown self-organization, and vegetation structure; 4) Soil carbon and nitrogen storage. In
940 this paper, we only evaluated the carbon cycle in the model simulations, though the nitrogen
941 cycle is also simulated in tandem with the carbon cycle in the model. We did not extensively
942 tune model parameters to fit observations because the purpose of this paper is to describe the
943 formulation of the model. The core processes of this model, e.g., photosynthesis, respiration,
944 phenology, growth, allocation, demography, soil biogeochemical cycles, are from well-

946 developed models and have been shown able to capture observational patterns. Data assimilation
947 approaches can be implemented when parameter tuning becomes essential.

948 The simulations demonstrate that this model can capture global patterns of GPP, LAI, tree
949 height, biomass, and soil carbon, even though the parameters are not extensively tuned. For
950 example, global GPP patterns are consistent with those derived from SIF data (Fig.7: a, b and
951 Fig. 8: a), and simulated tree heights span the same ranges of those derived from data. The
952 simulated biomass and soil carbon is generally higher than in observations, though simulated soil
953 carbon is lower in some cold regions. Several factors likely explain the apparent overestimates of
954 GPP, biomass, and soil carbon in the model. First, the model uses a potential PFT distribution
955 and does not account for land cover change and land use history. For example, carbon dense
956 ecosystems (e.g., forests) have been extensively replaced by croplands and pastures. Second,
957 while vegetation in the real world reflects a variety of successional stages and the effect of
958 various disturbance events, our model analyses are based on equilibrium simulations without
959 explicit disturbances, such as fire, deforestation and regrowth. Third, the model assumes mineral
960 nitrogen is saturated and can consistently meet demands for plant growth. We did not fix the land
961 cover mismatches by compromising ecosystem physiological processes because we cannot put
962 all these effects into current model structure (i.e., mortality) when many processes are missing.

963 LAI is an illustrative variable for understanding why compromises are necessary when
964 integrating ecologically based vegetation models into ESMs. LAI, as a critical prognostic
965 variable in vegetation models, links both plant physiology and biogeophysical interactions with
966 climate systems. While LAI is usually simulated by a fixed allocation scheme, even if the
967 allocation ratios are dynamic with vegetation productivity (Montané et al., 2017), the prediction
968 of LAI in models is often simplified as the balance between growth and turnover. Modelers tend

Deleted:

970 to tune LAI to fit observations and get the required albedo and water fluxes whatever their
 971 parameters of photosynthesis and respirations are. This LAI usually makes the lower layer
 972 leaves carbon negative. However, a first principle is that a tree should have an optimal LAI to
 973 maximize its carbon gain as a result of crown structure, light interception, and community-level
 974 competition (Anten, 2002; Hikosaka and Anten, 2012; Niinemets and Anten, 2009). Thus, in our
 975 model, because of the assumption of the uniform leaves within a crown, we defined a much
 976 small target LAI to avoid carbon negative leaves.

977 The “uniform leaf” assumption makes the lower layer leaves carbon negative when LAI is
 978 tuned close to that observed in tropical and boreal evergreen forests (where LAI is around 5~7).
 979 Therefore, the photosynthesis rate must be tuned to fit the canopy photosynthesis by keeping the
 980 carbon negative leaves. However, the carbon negative leaves do not affect ecosystem dynamics
 981 in the “single-cohort” models because the whole canopy net carbon gain is still reasonable and
 982 can be fitted to the observed dynamics. This contrasts with the demographic version of the
 983 model, which represents trees with different sizes and in different layers and creates conditions
 984 where seedlings in the understory cannot survive because of light limitation and negative carbon
 985 balances in some dry and cold regions. The leaf traits in the crown profile should, in reality, be a
 986 function of light, water and nitrogen (Niinemets et al., 2015). A more complex crown
 987 development module will then be required to simulate branching and leaf development and
 988 deployment processes. Modelers should balance the model complexity and computing efficiency
 989 then.

990 The leaf maximum carboxylation rate (V_{cmax}) used in this model is also much lower than
 991 measured in young leaves (Bonan et al., 2011) because the aging of leaves is considered in the
 992 mean value of V_{cmax} of all leaves with different ages. The mean V_{cmax} of the whole canopy leaves

Deleted:

Deleted: lower

Deleted:

Deleted: due to the assumption of the uniform the leaves within a crown

Deleted: The leaf traits in the crown profile should, in reality, be a function of light, water and nitrogen (Niinemets et al., 2015).

Deleted: is

Deleted: Thus

Deleted:

Deleted: more complex

1006 is much lower than the new leaves that are usually used to measure V_{cmax} . If the leaves were not
1007 specifically chosen, the mean of measured V_{cmax} is much lower than those used in models as
1008 shown in Verryckt et al. (2022). This also indicates that V_{cmax} in current vegetation models is
1009 over-estimated.

1010 The allometry of plant architecture, rules for plant growth, and reproduction and mortality
1011 processes form the basis of vegetation structural dynamics. The formulation of allometry makes
1012 the whole-tree's photosynthesis and respiration proportional to crown area, and thus the growth
1013 rate of tree diameter independent of crown area. The allocation scheme between the growth of
1014 stems and functional tissues (i.e., leaves and fine roots) is the strategy of resources foraging for
1015 light and soil resources, including height-structured competition for light.

1016 The vital rates drive vegetation structural changes and biogeochemical cycles (Purves et al.,
1017 2008). Our model makes it possible to simulate vegetation composition and structural dynamics
1018 based on the fundamental principles of ecology, and the transient changes in terrestrial
1019 ecosystems in response to climate change. This model therefore has the potential to predict
1020 competitively dominant strategies represented by plastic plant traits (e.g., competitively
1021 dominant LMA in the simulations of Fig. 13), and the vegetation structure and composition that
1022 will be eco-evolutionarily optimized.

1024 5.3 Major uncertainties in BiomeE

1025 Global vegetation models typically require simplifying assumptions to organize ecosystem
1026 processes at different scales into a cohesive model structure that balances the complexity of
1027 ecosystem processes and the limitations of our knowledge. In our model, many processes,

Deleted: ¶

The allometry of plant architecture, rules for plant growth, and reproduction and mortality processes form the basis of vegetation structural dynamics. The formulation of allometry makes the whole-tree's photosynthesis and respiration proportional to crown area, and thus the growth rate of tree diameter independent of crown area. These vital rates drive vegetation structural changes and biogeochemical cycles (Purves et al., 2008). Our model makes it possible to simulate vegetation composition and structural dynamics based on the fundamental principles of ecology, and the transient changes in terrestrial ecosystems in response to climate change. This model therefore has the potential to predict competitively dominant strategies represented by plastic plant traits (e.g., leaf traits, allocation etc.), resulting in simulated vegetation structure and composition that will be eco-evolutionarily optimized. PPA defines the height-structured competition for light. The allocation scheme between the growth of stems and functional tissues (i.e., leaves and fine roots) is the strategy of resources foraging for light and soil resources. ¶

Deleted: this model

Deleted:

Deleted: We used many

Deleted: Normally, a

Deleted: g

including phenology and drought effects, are based on phenomenological equations representing the poorly understood links between processes needed by the model to simulate the entire system. In the following sections, we highlight these assumptions and evaluate their relative benefits and costs. Transparency in the description of a community model such as this one will help future developers understand compromises and areas that can be improved with new information or approaches. The following phenomenological relationships represent the major sources of uncertainty in this model.

Water limitation of photosynthesis is calculated as a function of relative soil moisture following the water stress function from Rodriguez-Iturbe et al. (1999):

$$\beta_D = \text{Min} \left(1.0, \max \left(\frac{s_D - s_{\min}}{s^* - s_{\min}}, 0.0 \right) \right), \quad (16)$$

The parameters s^* and s_{\min} are PFT-specific, representing different responses of PFTs to soil water conditions, and s_D is the relative soil moisture ranging from 0 (soil water content at wilting point) to 1 (at field capacity). This formulation that scales soil moisture to a scalar between zero to 1 is repeatedly used in both physiological responses of photosynthesis and phenology in ecosystem models as a simplistic treatment of the central role of water limitation on plant physiology (Harper et al., 2021; De Kauwe et al., 2015; Powell et al., 2013). This equation does not include the detailed processes of plant hydraulics and its adaptation to arid environments.

Plants have multiple tradeoffs and strategies to improve their competitiveness under water stress, such as regulating stomata conductance, shedding leaves, producing more roots, etc. (Oliveira et al., 2021; Volaire, 2018). At the ecosystem level, competition and evolutionary processes filter community emergent properties (Franklin et al., 2020; van der Molen et al., 2011). For example, trees in different climate regions have similar hydraulic safety margins

Deleted: Gs typically simplifying assumptions to organize ecosystem processes at different scales into a cohesive model structure that balances the complexity of different processes and the sour knowledge. In our model, processes, including phenology, drought effects, are

1082 (Choat et al., 2012), partly due to the intense competition for light (height growth) and water
1083 (root allocation) that require optimal use of available resources at any climate conditions
1084 (Gleason et al., 2017; Liu et al., 2019). However, in this model, the drought responses are only
1085 delineated by Eq. 16. The parameter choices for s^* and s_{\min} likely explain the amplified water
1086 stresses and low productivity in arid regions within our model.

1087 Phenology represents the seasonal rhythms of plant physiological activities as adapted to
1088 periodic changes in temperature, precipitation, and light availability (Abramoff and Finzi, 2015;
1089 Caldararu et al., 2014; Chuine, 2010). DGVMs normally simulate leaf onset and senescence
1090 based on temperature conditions for cold deciduous plants and soil water conditions for drought
1091 deciduous plants (Arora and Boer, 2005; Caldararu et al., 2014). Phenology modeling is still
1092 highly empirical, although new models and approaches for cold deciduous and drought
1093 deciduous strategies have been proposed recently (e.g., Caldararu et al., 2014; Chen et al., 2016;
1094 Dahlin et al., 2015; Manzon et al., 2015). We used a simple formulation of temperature (Eqs 1
1095 and 3) and drought responses. For the cold-deciduous strategies, the phenology model balances
1096 growing season length and frost risks by adjusting critical GDD0 and T0 according to chilling
1097 days and growing days to reduce frost risk in warm regions and increase growing season length
1098 in cold regions. In this way, leaf senescence also considers growing season length and leaf aging.
1099 For example, in areas with longer growing seasons, plants will have a higher T0 and initiate
1100 senescence at higher temperatures. For the drought phenology, we set different critical soil
1101 moisture indexes to initiate and terminate a growing season (Table 1). However, these
1102 relationships are phenomenological, and ecological rules will benefit future model development.

1103 Mortality is an integrative result of accumulative physiological stresses, structural
1104 damages, and disturbances during a tree's lifetime. The direct reasons can be starvation,

1105 structural failure, hydraulic failure, etc. (McDowell, 2011; Aakala et al., 2012; Aleixo et al.,
1106 2019). In this model, we only consider the background mortality and define its rate as a function
1107 of tree diameter and light environment (Eq. 10). Hydraulic failure-induced mortality is required
1108 for studying plant responses to climate changes.

1109 We employed these general phenomenological equations primarily because more
1110 mechanistic equations are not currently known. We are using the key variables that characterize
1111 ecosystem properties to define the basic model structure but have to use less-than-solid
1112 information to link them together by phenomenological relationships, as all the models do. In
1113 addition, our interest is to keep this model as simple as possible to improve interpretability and
1114 transparency and to reduce the computational burden when it is integrated into the ModelE. In
1115 these places where the tradeoff between model complexity and process accuracy is necessary, we
1116 highlight the underlying assumptions clearly, rather than implementing temporary fixes that lack
1117 solid ecological principles.

Deleted: ¶

Deleted:

Deleted: than applying temporary fixes not based on solid ecological modeling approaches

Deleted: ¶

Deleted:

1119 5.4 Insights from comparison with MsTMIP model

1120 Most of the MsTMIP participant models have been analyzed by a model traceability method
1121 developed by Xia et al. (2013), which hierarchically decomposes model behavior into some
1122 fundamental processes of ecosystem carbon dynamics, such as GPP, carbon use efficiency
1123 (CUE), allocation coefficients, carbon residence time, carbon storage capacity, and
1124 environmental response functions (Zhou et al., 2021; Xia et al., 2013; Luo and Weng, 2011).
1125 This method is based on the assumptions of the linear system and the ecosystem emergent
1126 behavior per se (Emanuel and Killough, 1984; Eriksson, 1971; Sierra et al., 2018; Luo et al.,
1127 2012), making it is consistent with the concepts that are used as the basis of ecosystem carbon

cycle models. The analyses of model traceability found, for the carbon cycle dynamics, the major uncertainty is from the modeling of the turnover rates (reciprocals of residence time) of vegetation and soil carbon pools (Jiang et al., 2017; Chen et al., 2015). From CMIP5 to CMIP6, the modeling of NPP has been greatly improved, while the ecosystem carbon residence time remains highly biased (Wei et al., 2022).

According to the concepts of this traceability analysis approach (Xia et al., 2013), BiomeE also has a high uncertainty in the modeling of residence times of vegetation and soil carbon pools, because the mortality is picked up from the global forest data and the SOC decomposition processes are highly simplified. These issues have been discussed in the section of “5.3 Major uncertainties in BiomeE”. These concepts (e.g., residence time, allocation coefficients) describe model emergent properties resulting from the underlying biological and ecological processes (i.e., micro-dynamics vs. macro-states). Fitting the emergent properties directly to improve model behavior is natural and convenient because many vegetation models are using these emergent properties (e.g., CUE, residence time, and allocation coefficients) to describe ecosystem processes in their formulations as a tradition of ecosystem modeling.

There are a couple of common and long-lasting issues in terrestrial ecosystem modeling, such as responses to warming, responses to atmospheric CO₂, drought stress effects, and vegetation compositional changes (Harrison et al., 2021; Franklin et al., 2020; Luo, 2007). These issues represent our knowledge gaps in ecosystem ecology. For modeling vegetation dynamics eco-evolutionarily, we need to use the fundamental ecological processes and unbreakable physical rules to simulate the emergent processes (e.g., Weng et al., 2019; Scheiter et al., 2013). With the design of vegetation modeling in the BiomeE, such as the explicit demographic processes, individual-based competition for different resources, and flexible trait combinations of

1157 PFTs, this model is able to predict some key emergent dynamics of ecosystems based on the
1158 underlying biological and evolutionary mechanisms (as shown in Figure 13). Data from field
1159 experiments (Ainsworth and Long, 2004; Crowther et al., 2016), observatory networks (e.g.,
1160 Fluxnet, Baldocchi et al., 2001; Friend et al., 2007), and remote sensing (Duncanson et al.,
1161 2020), can provide direct information for modeling the underlying ecological processes and
1162 validating predicted emergent properties.

1163
1164 **5.5 Model stability and complexity**

1165 Ecosystem demographic processes (e.g., reproduction and mortality) are a source of high
1166 sensitivity and uncertainty in BiomeE. In some environmental conditions, especially in dry or
1167 cold regions, the predefined parameters can lead to high mortality or failure of reproduction,
1168 making ecosystems highly instable. To understand these issues, we developed a “single-cohort”
1169 version of the model to aid in the diagnosis of issues in the full demographic version of the
1170 model. The major issue we identified is the fact that the model formulation is based on functional
1171 processes in highly-productive regions, whereas the model is applied globally and across much
1172 more diverse environmental conditions (e.g., arid environments). The variables and parameters
1173 that work well in highly-productive regions (e.g., initial seedling sizes, default leaf growth,
1174 minimum allocation ratios, etc.) are often unsuitable in regions with higher environmental stress.
1175 And although plants have evolved special features to deal with more extreme conditions (Lloret
1176 et al., 2012; Reyser et al., 2013; Singh et al., 2020), these features have not yet been integrated
1177 into the model.

1178 There is a tendency in current DGVMs to use individual plant physiological trait changes
1179 to represent community shifts. This approach is usually characterized as “parameter dynamics”

Deleted: Data from field experiments (Ainsworth and Long, 2004; Crowther et al., 2016), observatory networks (Baldocchi et al., 2001), and remote sensing (Duncanson et al., 2020), provide direct information for the modeling of the underlying ecological processes

Formatted: Indent: First line: 0", Line spacing: Multiple 1.15 li

Deleted: (Zhou et al., 2021)(Jiang et al., 2017; Yizhao et al., 2015)(Wei et al., 2022)(Xia et al., 2013)

Deleted: .

Deleted: ¶

5.4 Model stability and complexity¶

Formatted: Font: Bold

Formatted: Indent: First line: 0"

Deleted: uniform

Deleted: leading to high instability of vegetation

1193 or “response functions” (Fisher and Koven, 2020) for reducing model processes and complexity.
1194 Adding new processes to work around existing problems, instead of redesigning the fundamental
1195 model processes, is common in model development. The approach is helpful for tracking model
1196 development, undoing wrong additions, and improving model performance. However, work-
1197 arounds often increase model complexity without concomitant improvements in model
1198 predictions.

1199 Generally, a model’s usefulness is improved by transparent assumptions, a well-defined
1200 model structure, and output that is testable against data (Famiglietti et al., 2021; Forster, 2017;
1201 Hourdin et al., 2017). Data assimilation approaches improve model parameterization more
1202 efficiently and effectively than manually tuning individual parameters (Williams et al., 2009;
1203 MacBean et al., 2016; Wang et al., 2009) and allow for more detailed uncertainty analysis (Luo
1204 et al., 2009; Weng et al., 2011; Weng and Luo, 2011; Xu et al., 2006; Dietze, 2014). It is
1205 important to only include necessary assumptions in a model and to include them in ways that do
1206 not compromise other processes or parameters. Modelers should try their best not to add poor-
1207 understood processes if not necessary. Additionally, many specifications of model formulation
1208 are based on the questions that a user is trying to answer in their research. We should not expect
1209 to develop an all-encompassing model that fits all application scenarios. On the contrary,
1210 maintaining model flexibility and transparency is critical for using this model as a tool to explore
1211 specific science questions. In BiomeE, we have opted for what we consider the most
1212 parsimonious and, at the same time, theoretically sound formulations of allometry, phenology,
1213 and allocation dynamics to allow for computational efficiency in capturing vegetation growth and
1214 ecological dynamics in the context of an ESM.

1215

1216 5.6 Legacy limitations of ModelE coding and development conventions

1217 The legacy of model coding structure and the history of model development can greatly affect
1218 the functions and the selection of model formulations (Alexander and Easterbrook, 2015).

1219 ModelE was developed as a general circulation model, and vegetation in the model to date has
1220 been represented with a simple set of static biophysics parameterizations to regulate exchanges
1221 of energy and moisture between the land surface and the atmosphere (i.e., a big leaf model)
1222 (Hansen et al., 2007; Schmidt et al., 2014; Kelley et al., 2020). To advance the functionality of
1223 the vegetation and the land surface model within ModelE, increases in complexity must therefore
1224 be balanced with the computational demands of the fully-coupled model.

1225 In ModelE, the land model, TerraE, is used to calculate land surface (including vegetation)
1226 water and energy fluxes and soil water dynamics based on the characteristics of vegetation
1227 derived from the vegetation model (e.g., canopy conductance, wetness, etc.) at the grid scale. It
1228 does not calculate each cohort's transpiration and water uptake. In our vegetation model, the
1229 water limitation of stomatal conductance is calculated as a function of soil water stress index and
1230 root vertical distribution, instead of the direct plant root water supply (plant hydraulics). This
1231 setting works well for the big leaf model (one canopy at one grid). However, when multiple
1232 cohorts of plants are represented in the model, as we do in BiomeE, it is unable to represent
1233 water competition and differentiate the contribution of each single cohort's contribution to the
1234 total transpiration. A structural change will be required to solve this problem by calculating
1235 transpiration from the bottom-up (i.e., from cohort up to grid cell).

1236
1237 **6 Conclusions**

Deleted: is

Formatted: Indent: First line: 0.38"

Deleted: ¶

Deleted: The legacy of model coding structure and the history of model development can greatly affect the functions and the selection of model formulations (Alexander and Easterbrook, 2015). When incorporating new processes, especially a new vegetation dynamic model, we must balance the stability requirement of the parent model and the risks of the model crashing. As shown in the comparison with the single cohort model (Fig. 11), the full demography setting has many potential failing points in regeneration in more extreme environmental conditions.

Deleted: ¶

1251 We developed a new demographic vegetation model to improve the representation of terrestrial
1252 vegetation dynamics and ecosystem biogeochemical cycles in the NASA Goddard Institute of
1253 Space Studies' coupled Earth system model, ModelE. This model includes the processes of plant
1254 growth, mortality, reproduction, vegetation structural dynamics, and soil carbon and nitrogen
1255 cycling. To scale this model globally, we added a new set of plant functional types to represent
1256 global vegetation functional diversity and introduced new phenology algorithms to deal with the
1257 seasonality of temperature and soil water availability. Competition for light and soil resources is
1258 individual-based, which makes the modeling of eco-evolutionary optimality possible. This model
1259 predicts the dynamics of vegetation and soil biogeochemistry including leaf area index,
1260 vegetation structure (e.g., height, tree density, size distribution, crown organization), and
1261 ecosystem carbon and nitrogen storage and fluxes. This model will enable ModelE to simulate
1262 long-term biogeophysical and biogeochemical feedbacks between the climate system and land
1263 ecosystems at decadal to century temporal scales. It will also allow for the prediction of transient
1264 vegetation dynamics and eco-evolutionary community assemblage in response to future climate
1265 changes based on the fundamental ecological principles.

1266

1267

1268 **Code and data availability**

1269 The model codes have been coupled with NASA GISS ModelE and will be released with
1270 ModelE codes (<https://www.giss.nasa.gov/tools/modelE/>). The codes of BiomeE module are
1271 available at <https://doi.org/10.5281/zenodo.6476152>. The simulated data have been archived at
1272 Zenodo (<https://doi.org/10.5281/zenodo.6480411>).

1273

1274 **Author contributions**

1275 EW coded the model and performed test runs and data analysis. EW and BIC wrote the first draft
1276 of the manuscript. BIC, MJP, SSM, NYK, and EW designed the functional coupling with
1277 ModelE and the land module. NYK, IA, RS, and MK contributed to input data, the IO structure
1278 and the coupling between BiomeE and ModelE. KW, RD, CE, and SWP contributed to
1279 conceptual model development and PFT design. All co-authors contributed to writing or
1280 improving the manuscript.

1281

1282 **Competing interests**

1283 The authors declare that they have no conflict of interest.

1284

1285 **Acknowledgements**

1286 This work was supported by NASA Modeling, Analysis, and Prediction (MAP) Program (award
1287 numbers: 80NSSC21K1496, NNN10ZDA001N, and 16-MAP16-0149). Computing resources for
1288 the model runs were provided by the NASA High-End Computing (HEC) Program through the
1289 NASA Center for Climate Simulation (NCCS) at Goddard Space Flight Center. We thank Dr.
1290 Pierre Gentine of Department of Earth and Environmental Engineering, Columbia University, for
1291 his help in GPP data and model validation.

1292

- Reference**
- Aakala, T., Fraver, S., Palik, B. J., and D'Amato, A. W.: Spatially random mortality in old-growth red pine forests of northern Minnesota, 42, 899–907, <https://doi.org/10.1139/x2012-044>, 2012.
- Abramoff, R. Z. and Finzi, A. C.: Are above- and below-ground phenology in sync?, 205, 1054–1061, <https://doi.org/10.1111/nph.13111>, 2015.
- Ainsworth, E. A. and Long, S. P.: What have we learned from 15 years of free-air CO₂ enrichment (FACE)? A meta-analytic review of the responses of photosynthesis, canopy properties and plant production to rising CO₂: Tansley review, 165, 351–372, <https://doi.org/10.1111/j.1469-8137.2004.01224.x>, 2004.
- Aleixo, I., Norris, D., Hemerik, L., Barbosa, A., Prata, E., Costa, F., and Poorter, L.: Amazonian rainforest tree mortality driven by climate and functional traits, 9, 384–388, <https://doi.org/10.1038/s41558-019-0458-0>, 2019.
- Alemohammad, S. H., Fang, B., Konings, A. G., Aires, F., Green, J. K., Kolassa, J., Miralles, D., Prigent, C., and Gentile, P.: Water, Energy, and Carbon with Artificial Neural Networks (WECANN): a statistically based estimate of global surface turbulent fluxes and gross primary productivity using solar-induced fluorescence, 14, 4101–4124, <https://doi.org/10.5194/bg-14-4101-2017>, 2017.
- Alexander, K. and Easterbrook, S. M.: The software architecture of climate models: a graphical comparison of CMIP5 and EMICAR5 configurations, 8, 1221–1232, <https://doi.org/10.5194/gmd-8-1221-2015>, 2015.
- Allen, C. D., Macalady, A. K., Chenchouni, H., Bachelet, D., McDowell, N., Vennetier, M., Kitzberger, T., Rigling, A., Breshears, D. D., Hogg, E. H. (Ted), Gonzalez, P., Fensham, R., Zhang, Z., Castro, J., Demidova, N., Lim, J.-H., Allard, G., Running, S. W., Semerci, A., and Cobb, N.: A global overview of drought and heat-induced tree mortality reveals emerging climate change risks for forests, 259, 660–684, <https://doi.org/10.1016/j.foreco.2009.09.001>, 2010.
- Anderegg, W. R. L., Kane, J. M., and Anderegg, L. D. L.: Consequences of widespread tree mortality triggered by drought and temperature stress, 3, 30–36, <https://doi.org/10.1038/nclimate1635>, 2012.
- Anten, N. P.: Evolutionarily stable leaf area production in plant populations, 217, 15–32, 2002.
- Argles, A. P. K., Moore, J. R., Huntingford, C., Wiltshire, A. J., Harper, A. B., Jones, C. D., and Cox, P. M.: Robust Ecosystem Demography (RED version 1.0): a parsimonious approach to modelling vegetation dynamics in Earth system models, 13, 4067–4089, <https://doi.org/10.5194/gmd-13-4067-2020>, 2020.
- Arora, V. K. and Boer, G. J.: A parameterization of leaf phenology for the terrestrial ecosystem component of climate models, 11, 39–59, <https://doi.org/10.1111/j.1365-2486.2004.00890.x>, 2005.
- Arora, V. K., Katavouta, A., Williams, R. G., Jones, C. D., Brovkin, V., Friedlingstein, P., Schwinger, J., Bopp, L., Boucher, O., Cadule, P., Chamberlain, M. A., Christian, J. R., Delire, C., Fisher, R. A., Hajima, T., Ilyina, T., Joetjzer, E., Kawamiya, M., Koven, C. D.,

Formatted: Font: Not Bold

Formatted: Indent: Left: 0", Hanging: 0.38", Space After: 6 pt

1334 Krasting, J. P., Law, R. M., Lawrence, D. M., Lenton, A., Lindsay, K., Pongratz, J.,
1335 Raddatz, T., Séférian, R., Tachiiri, K., Tjiputra, J. F., Wiltshire, A., Wu, T., and Ziehn, T.:
1336 Carbon-concentration and carbon-climate feedbacks in CMIP6 models and their
1337 comparison to CMIP5 models, 17, 4173–4222, <https://doi.org/10.5194/bg-17-4173-2020>,
1338 2020.

1339 Avissar, R. and Werth, D.: Global Hydroclimatological Teleconnections Resulting from Tropical
1340 Deforestation, *J. Hydrometeor.*, 6, 134–145, <https://doi.org/10.1175/JHM406.1>, 2005.

1341 Baldocchi, D., Falge, E., Gu, L., Olson, R., Hollinger, D., Running, S., Anthoni, P., Bernhofer,
1342 C., Davis, K., Evans, R., Fuentes, J., Goldstein, A., Katul, G., Law, B., Lee, X., Malhi, Y.,
1343 Meyers, T., Munger, W., Oechel, W., Paw U, K. T., Pilegaard, K., Schmid, H. P.,
1344 Valentini, R., Verma, S., Vesala, T., Wilson, K., and Wofsy, S.: FLUXNET: A New Tool
1345 to Study the Temporal and Spatial Variability of Ecosystem-Scale Carbon Dioxide, Water
1346 Vapor, and Energy Flux Densities, *Bull. Amer. Meteor. Soc.*, 82, 2415–2434,
1347 [https://doi.org/10.1175/1520-0477\(2001\)082<2415:FANTTS>2.3.CO;2](https://doi.org/10.1175/1520-0477(2001)082<2415:FANTTS>2.3.CO;2), 2001.

1348 Bonan, G. B., Lawrence, P. J., Oleson, K. W., Levis, S., Jung, M., Reichstein, M., Lawrence, D.
1349 M., and Swenson, S. C.: Improving canopy processes in the Community Land Model
1350 version 4 (CLM4) using global flux fields empirically inferred from FLUXNET data, 116,
1351 <https://doi.org/10.1029/2010JG001593>, 2011.

1352 Brando, P. M., Paolucci, L., Ummenhofer, C. C., Ordway, E. M., Hartmann, H., Cattau, M. E.,
1353 Rattis, L., Medjibe, V., Coe, M. T., and Balch, J.: Droughts, Wildfires, and Forest Carbon
1354 Cycling: A Pantropical Synthesis, *Annu. Rev. Earth Planet. Sci.*, 47, 555–581,
1355 <https://doi.org/10.1146/annurev-earth-082517-010235>, 2019.

1356 Briones, M. J. I., McNamara, N. P., Poskitt, J., Crow, S. E., and Ostle, N. J.: Interactive biotic
1357 and abiotic regulators of soil carbon cycling: evidence from controlled climate experiments
1358 on peatland and boreal soils, 20, 2971–2982, <https://doi.org/10.1111/gcb.12585>, 2014.

1359 Brodribb, T. J., Powers, J., Cochard, H., and Choat, B.: Hanging by a thread? Forests and
1360 drought, 368, 261–266, <https://doi.org/10.1126/science.aat7631>, 2020.

1361 Caldararu, S., Purves, D. W., and Palmer, P. I.: Phenology as a strategy for carbon optimality: a
1362 global model, 11, 763–778, <https://doi.org/10.5194/bg-11-763-2014>, 2014.

1363 Chave, J., Coomes, D., Jansen, S., Lewis, S. L., Swenson, N. G., and Zanne, A. E.: Towards a
1364 worldwide wood economics spectrum, 12, 351–366, <https://doi.org/10.1111/j.1461-0248.2009.01285.x>, 2009.

1366 Chen, M., Melaas, E. K., Gray, J. M., Friedl, M. A., and Richardson, A. D.: A new seasonal-
1367 deciduous spring phenology submodel in the Community Land Model 4.5: impacts on
1368 carbon and water cycling under future climate scenarios, 22, 3675–3688,
1369 <https://doi.org/10.1111/gcb.13326>, 2016.

1370 Choat, B., Jansen, S., Brodribb, T. J., Cochard, H., Delzon, S., Bhaskar, R., Bucci, S. J., Feild, T.
1371 S., Gleason, S. M., Hacke, U. G., Jacobsen, A. L., Lens, F., Maherali, H., Martínez-Vilalta,
1372 J., Mayr, S., Mencuccini, M., Mitchell, P. J., Nardini, A., Pittermann, J., Pratt, R. B.,
1373 Sperry, J. S., Westoby, M., Wright, I. J., and Zanne, A. E.: Global convergence in the
1374 vulnerability of forests to drought, <https://doi.org/10.1038/nature11688>, 2012.

1375 Chuine, I.: Why does phenology drive species distribution?, 365, 3149–3160,
1376 <https://doi.org/10.1098/rstb.2010.0142>, 2010.

1377 Clark, J. S., Iverson, L., Woodall, C. W., Allen, C. D., Bell, D. M., Bragg, D. C., D’Amato, A.
1378 W., Davis, F. W., Hersh, M. H., Ibanez, I., Jackson, S. T., Matthews, S., Pederson, N.,
1379 Peters, M., Schwartz, M. W., Waring, K. M., and Zimmermann, N. E.: The impacts of
1380 increasing drought on forest dynamics, structure, and biodiversity in the United States, 22,
1381 2329–2352, <https://doi.org/10.1111/gcb.13160>, 2016.

1382 Crowther, T. W., Todd-Brown, K. E. O., Rowe, C. W., Wieder, W. R., Carey, J. C., Machmuller,
1383 M. B., Snoek, B. L., Fang, S., Zhou, G., Allison, S. D., Blair, J. M., Bridgham, S. D.,
1384 Burton, A. J., Carrillo, Y., Reich, P. B., Clark, J. S., Classen, A. T., Dijkstra, F. A.,
1385 Elberling, B., Emmett, B. A., Estiarte, M., Frey, S. D., Guo, J., Harte, J., Jiang, L., Johnson,
1386 B. R., Kröel-Dulay, G., Larsen, K. S., Laudon, H., Lavalley, J. M., Luo, Y., Lupascu, M.,
1387 Ma, L. N., Marhan, S., Michelsen, A., Mohan, J., Niu, S., Pendall, E., Peñuelas, J., Pfeifer-
1388 Meister, L., Poll, C., Reinsch, S., Reynolds, L. L., Schmidt, I. K., Sistla, S., Sokol, N. W.,
1389 Templer, P. H., Treseder, K. K., Welker, J. M., and Bradford, M. A.: Quantifying global
1390 soil carbon losses in response to warming, 540, 104–108,
1391 <https://doi.org/10.1038/nature20150>, 2016.

1392 Dahlin, K. M., Fisher, R. A., and Lawrence, P. J.: Environmental drivers of drought deciduous
1393 phenology in the Community Land Model, 12, 5061–5074, <https://doi.org/10.5194/bg-12-5061-2015>, 2015.

1395 Davidson, E. A. and Janssens, I. A.: Temperature sensitivity of soil carbon decomposition and
1396 feedbacks to climate change, *Nature*, 440, 165–173, <https://doi.org/10.1038/nature04514>,
1397 2006.

1398 De Kauwe, M. G., Zhou, S.-X., Medlyn, B. E., Pitman, A. J., Wang, Y.-P., Duursma, R. A., and
1399 Prentice, I. C.: Do land surface models need to include differential plant species responses
1400 to drought? Examining model predictions across a mesic-xeric gradient in Europe, 12,
1401 7503–7518, <https://doi.org/10.5194/bg-12-7503-2015>, 2015.

1402 Dieckmann, U., Brannstrom, A., HilleRisLambes, R., and Ito, H. C.: The Adaptive Dynamics of
1403 Community Structure, in: *Mathematics for Ecology and Environmental Sciences*, edited
1404 by: Takeuchi, Yasuhiro, Iwasa, Yoh, and Sato, Kazunori, Springer, 145–177, 2007.

1405 Dietze, M. C.: Gaps in knowledge and data driving uncertainty in models of photosynthesis, 119,
1406 3–14, <https://doi.org/10.1007/s11120-013-9836-z>, 2014.

1407 Duncanson, L., Neuenschwander, A., Hancock, S., Thomas, N., Fatoyinbo, T., Simard, M.,
1408 Silva, C. A., Armston, J., Luthcke, S. B., Hofton, M., Kellner, J. R., and Dubayah, R.:
1409 Biomass estimation from simulated GEDI, ICESat-2 and NISAR across environmental
1410 gradients in Sonoma County, California, *Remote Sensing of Environment*, 242, 111779,
1411 <https://doi.org/10.1016/j.rse.2020.111779>, 2020.

1412 Dyzbinski, R., Farrior, C., Wolf, A., Reich, P. B., and Pacala, S. W.: Evolutionarily Stable
1413 Strategy Carbon Allocation to Foliage, Wood, and Fine Roots in Trees Competing for
1414 Light and Nitrogen: An Analytically Tractable, Individual-Based Model and Quantitative
1415 Comparisons to Data, 177, 153–166, <https://doi.org/10.1086/657992>, 2011.

- 1416 Dybzinski, R., Farrior, C. E., and Pacala, S. W.: Increased forest carbon storage with increased
1417 atmospheric CO₂ despite nitrogen limitation: a game-theoretic allocation model for trees in
1418 competition for nitrogen and light, 21, 1182–1196, <https://doi.org/10.1111/gcb.12783>,
1419 2015.
- 1420 Euskirchen, E. S., Edgar, C. W., Turetsky, M. R., Waldrop, M. P., and Harden, J. W.:
1421 Differential response of carbon fluxes to climate in three peatland ecosystems that vary in
1422 the presence and stability of permafrost, 119, 1576–1595,
1423 <https://doi.org/10.1002/2014JG002683>, 2014.
- 1424 Falster, D. and Westoby, M.: Plant height and evolutionary games, 18, 337–343,
1425 [https://doi.org/10.1016/S0169-5347\(03\)00061-2](https://doi.org/10.1016/S0169-5347(03)00061-2), 2003.
- 1426 Falster, D. S., Braennstroem, A., Westoby, M., and Dieckmann, U.: Multitrait successional forest
1427 dynamics enable diverse competitive coexistence, 114, E2719–E2728,
1428 <https://doi.org/10.1073/pnas.1610206114>, 2017.
- 1429 Famiglietti, C. A., Smallman, T. L., Levine, P. A., Flack-Prain, S., Quetin, G. R., Meyer, V.,
1430 Parazoo, N. C., Stettz, S. G., Yang, Y., Bonal, D., Bloom, A. A., Williams, M., and
1431 Konings, A. G.: Optimal model complexity for terrestrial carbon cycle prediction, 18,
1432 2727–2754, <https://doi.org/10.5194/bg-18-2727-2021>, 2021.
- 1433 Farrior, C. E.: Theory predicts plants grow roots to compete with only their closest neighbours,
1434 *Proceedings of the Royal Society B: Biological Sciences*, 286, 20191129,
1435 <https://doi.org/10.1098/rspb.2019.1129>, 2019.
- 1436 Farrior, C. E., Dybzinski, R., Levin, S. A., and Pacala, S. W.: Competition for Water and Light
1437 in Closed-Canopy Forests: A Tractable Model of Carbon Allocation with Implications for
1438 Carbon Sinks, 181, 314–330, <https://doi.org/10.1086/669153>, 2013.
- 1439 Fisher, R. A. and Koven, C. D.: Perspectives on the Future of Land Surface Models and the
1440 Challenges of Representing Complex Terrestrial Systems, 12, e2018MS001453,
1441 <https://doi.org/10.1029/2018MS001453>, 2020.
- 1442 Fisher, R. A., Muszala, S., Versteinstein, M., Lawrence, P., Xu, C., McDowell, N. G., Knox, R.
1443 G., Koven, C., Holm, J., Rogers, B. M., Spessa, A., Lawrence, D., and Bonan, G.: Taking
1444 off the training wheels: the properties of a dynamic vegetation model without climate
1445 envelopes, *CLM4.5(ED)*, 8, 3593–3619, <https://doi.org/10.5194/gmd-8-3593-2015>, 2015.
- 1446 von Foerster, H.: Some remarks on changing populations, in: *The kinetics of cellular proliferation*,
1447 edited by: Stohman, F., Grune and Stratton, New York, 382–407, 1959.
- 1448 Forster, P.: Half a century of robust climate models, 545, 296–297,
1449 <https://doi.org/10.1038/545296a>, 2017.
- 1450 Franklin, O., Johansson, J., Dewar, R. C., Dieckmann, U., McMurtrie, R. E., Brannstrom, A., and
1451 Dybzinski, R.: Modeling carbon allocation in trees: a search for principles, 32, 648–666,
1452 <https://doi.org/10.1093/treephys/tpr138>, 2012.
- 1453 Franklin, O., Harrison, S. P., Dewar, R., Farrior, C. E., Brännström, Å., Dieckmann, U., Pietsch,
1454 S., Falster, D., Cramer, W., Loreau, M., Wang, H., Mäkelä, A., Rebel, K. T., Meron, E.,
1455 Schymanski, S. J., Rovenskaya, E., Stocker, B. D., Zaehle, S., Manzoni, S., van Oijen, M.,
1456 Wright, I. J., Ciais, P., van Bodegom, P. M., Peñuelas, J., Hofhansl, F., Terrer, C.,

1457 Soudzilovskaia, N. A., Midgley, G., and Prentice, I. C.: Organizing principles for
1458 vegetation dynamics, 1–10, <https://doi.org/10.1038/s41477-020-0655-x>, 2020.

1459 Friedl, M. A., Sulla-Menashe, D., Tan, B., Schneider, A., Ramankutty, N., Sibley, A., and
1460 Huang, X.: MODIS Collection 5 global land cover: Algorithm refinements and
1461 characterization of new datasets, 114, 168–182, <https://doi.org/10.1016/j.rse.2009.08.016>,
1462 2010.

1463 Friedlingstein, P., Meinshausen, M., Arora, V. K., Jones, C. D., Anav, A., Liddicoat, S. K., and
1464 Knutti, R.: Uncertainties in CMIP5 Climate Projections due to Carbon Cycle Feedbacks,
1465 27, 511–526, <https://doi.org/10.1175/JCLI-D-12-00579.1>, 2014.

1466 Friend, A. D., Stevens, A. K., Knox, R. G., and Cannell, M. G. R.: A process-based, terrestrial
1467 biosphere model of ecosystem dynamics (Hybrid v3.0), *Ecological Modelling*, 95, 249–
1468 287, [https://doi.org/10.1016/S0304-3800\(96\)00034-8](https://doi.org/10.1016/S0304-3800(96)00034-8), 1997.

1469 Fu, Z., Li, D., Hararuk, O., Schwalm, C., Luo, Y., Yan, L., and Niu, S.: Recovery time and state
1470 change of terrestrial carbon cycle after disturbance, *Environ. Res. Lett.*, 12, 104004,
1471 <https://doi.org/10.1088/1748-9326/aa8a5c>, 2017.

1472 Garcia, E. S., Swann, A. L. S., Villegas, J. C., Breshears, D. D., Law, D. J., Saleska, S. R., and
1473 Stark, S. C.: Synergistic Ecoclimate Teleconnections from Forest Loss in Different Regions
1474 Structure Global Ecological Responses, *PLoS One*, 11,
1475 <https://doi.org/10.1371/journal.pone.0165042>, 2016.

1476 Gleason, K. E., Bradford, J. B., Bottero, A., D’Amato, A. W., Fraver, S., Palik, B. J., Battaglia,
1477 M. A., Iverson, L., Kenefic, L., and Kern, C. C.: Competition amplifies drought stress in
1478 forests across broad climatic and compositional gradients, 8, e01849,
1479 <https://doi.org/10.1002/ecs2.1849>, 2017.

1480 Green, J. K., Konings, A. G., Alemohammad, S. H., Berry, J., Entekhabi, D., Kolassa, J., Lee, J.-
1481 E., and Gentine, P.: Regionally strong feedbacks between the atmosphere and terrestrial
1482 biosphere, *Nature Geosci.*, 10, 410–414, <https://doi.org/10.1038/ngeo2957>, 2017.

1483 Hansen, J., Sato, M., Ruedy, R., Kharecha, P., Lacis, A., Miller, R., Nazarenko, L., Lo, K.,
1484 Schmidt, G. A., Russell, G., Aleinov, I., Bauer, S., Baum, E., Cairns, B., Canuto, V.,
1485 Chandler, M., Cheng, Y., Cohen, A., Del Genio, A., Faluvegi, G., Fleming, E., Friend, A.,
1486 Hall, T., Jackman, C., Jonas, J., Kelley, M., Kiang, N. Y., Koch, D., Labow, G., Lerner, J.,
1487 Menon, S., Novakov, T., Oinas, V., Perlwitz, Ja., Perlwitz, Ju., Rind, D., Romanou, A.,
1488 Schmunk, R., Shindell, D., Stone, P., Sun, S., Streets, D., Tausnev, N., Thresher, D.,
1489 Unger, N., Yao, M., and Zhang, S.: Climate simulations for 1880–2003 with GISS modelE,
1490 29, 661–696, <https://doi.org/10.1007/s00382-007-0255-8>, 2007.

1491 Harper, A. B., Williams, K. E., McGuire, P. C., Duran Rojas, M. C., Hemming, D., Verhoef, A.,
1492 Huntingford, C., Rowland, L., Marthews, T., Breder Eller, C., Mathison, C., Nobrega, R. L.
1493 B., Gedney, N., Vidale, P. L., Otu-Larbi, F., Pandey, D., Garrigues, S., Wright, A., Slevin,
1494 D., De Kauwe, M. G., Blyth, E., Ardö, J., Black, A., Bonal, D., Buchmann, N., Burban, B.,
1495 Fuchs, K., de Grandcourt, A., Mammarella, I., Merbold, L., Montagnani, L., Nouvellon, Y.,
1496 Restrepo-Coupe, N., and Wohlfahrt, G.: Improvement of modeling plant responses to low
1497 soil moisture in JULESv4.9 and evaluation against flux tower measurements, 14, 3269–
1498 3294, <https://doi.org/10.5194/gmd-14-3269-2021>, 2021.

- 1499 Harrison, S. P., Cramer, W., Franklin, O., Prentice, I. C., Wang, H., Brännström, Å., de Boer, H.,
1500 Dieckmann, U., Joshi, J., Keenan, T. F., Lavergne, A., Manzoni, S., Mengoli, G.,
1501 Morfopoulos, C., Peñuelas, J., Pietsch, S., Rebel, K. T., Ryu, Y., Smith, N. G., Stocker, B.
1502 D., and Wright, I. J.: Eco-evolutionary optimality as a means to improve vegetation and
1503 land-surface models, 231, 2125–2141, <https://doi.org/10.1111/nph.17558>, 2021.
- 1504 Hengeveld, G. M., Gunia, K., Didion, M., Zudin, S., Clercx, A. P. P. M., and Schelhaas, M. J.:
1505 Global 1-degree Maps of Forest Area, Carbon Stocks, and Biomass, 1950-2010, ,
1506 <https://doi.org/10.3334/ORNLDAAAC/1296>, 2015.
- 1507 Hikosaka, K. and Anten, N. P. R.: An evolutionary game of leaf dynamics and its consequences
1508 for canopy structure, 26, 1024–1032, <https://doi.org/10.1111/j.1365-2435.2012.02042.x>,
1509 2012.
- 1510 Hourdin, F., Mauritsen, T., Gettelman, A., Golaz, J.-C., Balaji, V., Duan, Q., Folini, D., Ji, D.,
1511 Klocke, D., Qian, Y., Rauser, F., Rio, C., Tomassini, L., Watanabe, M., and Williamson,
1512 D.: The Art and Science of Climate Model Tuning, 98, 589–602,
1513 <https://doi.org/10.1175/BAMS-D-15-00135.1>, 2017.
- 1514 Huang, M., Piao, S., Sun, Y., Ciais, P., Cheng, L., Mao, J., Poulter, B., Shi, X., Zeng, Z., and
1515 Wang, Y.: Change in terrestrial ecosystem water-use efficiency over the last three decades,
1516 21, 2366–2378, <https://doi.org/10.1111/gcb.12873>, 2015.
- 1517 Huntzinger, D. N., Post, W. M., Wei, Y., Michalak, A. M., West, T. O., Jacobson, A. R., Baker,
1518 I. T., Chen, J. M., Davis, K. J., Hayes, D. J., Hoffman, F. M., Jain, A. K., Liu, S., McGuire,
1519 A. D., Neilson, R. P., Potter, C., Poulter, B., Price, D., Raczka, B. M., Tian, H. Q.,
1520 Thornton, P., Tomelleri, E., Viovy, N., Xiao, J., Yuan, W., Zeng, N., Zhao, M., and Cook,
1521 R.: North American Carbon Program (NACP) regional interim synthesis: Terrestrial
1522 biospheric model intercomparison, 232, 144–157,
1523 <https://doi.org/10.1016/j.ecolmodel.2012.02.004>, 2012.
- 1524 Huntzinger, D. N., Schwalm, C., Michalak, A. M., Schaefer, K., King, A. W., Wei, Y., Jacobson,
1525 A., Liu, S., Cook, R. B., Post, W. M., Berthier, G., Hayes, D., Huang, M., Ito, A., Lei, H.,
1526 Lu, C., Mao, J., Peng, C. H., Peng, S., Poulter, B., Riccuto, D., Shi, X., Tian, H., Wang,
1527 W., Zeng, N., Zhao, F., and Zhu, Q.: The North American Carbon Program Multi-Scale
1528 Synthesis and Terrestrial Model Intercomparison Project – Part 1: Overview and
1529 experimental design, 6, 2121–2133, <https://doi.org/10.5194/gmd-6-2121-2013>, 2013.
- 1530 Ito, G., Romanou, A., Kiang, N. Y., Faluvegi, G., Aleinov, I., Ruedy, R., Russell, G., Lerner, P.,
1531 Kelley, M., and Lo, K.: Global Carbon Cycle and Climate Feedbacks in the NASA GISS
1532 ModelE2.1, 12, e2019MS002030, <https://doi.org/10.1029/2019MS002030>, 2020.
- 1533 Jiang, L., Shi, Z., Xia, J., Liang, J., Lu, X., Wang, Y., and Luo, Y.: Transient Traceability
1534 Analysis of Land Carbon Storage Dynamics: Procedures and Its Application to Two Forest
1535 Ecosystems, 9, 2822–2835, <https://doi.org/10.1002/2017MS001004>, 2017.
- 1536 Keenan, T. F., Hollinger, D. Y., Bohrer, G., Dragoni, D., Munger, J. W., Schmid, H. P., and
1537 Richardson, A. D.: Increase in forest water-use efficiency as atmospheric carbon dioxide
1538 concentrations rise, 499, 324–327, <https://doi.org/10.1038/nature12291>, 2013.
- 1539 Kelley, M., Schmidt, G. A., Nazarenko, L. S., Bauer, S. E., Ruedy, R., Russell, G. L., Ackerman,
1540 A. S., Aleinov, I., Bauer, M., Bleck, R., Canuto, V., Cesana, G., Cheng, Y., Clune, T. L.,

1541 Cook, B. I., Cruz, C. A., Del Genio, A. D., Elsaesser, G. S., Faluvegi, G., Kiang, N. Y.,
 1542 Kim, D., Laci, A. A., Leboissetier, A., LeGrande, A. N., Lo, K. K., Marshall, J.,
 1543 Matthews, E. E., McDermid, S., Mezuman, K., Miller, R. L., Murray, L. T., Oinas, V.,
 1544 Orbe, C., García-Pando, C. P., Perlwitz, J. P., Puma, M. J., Rind, D., Romanou, A.,
 1545 Shindell, D. T., Sun, S., Tausnev, N., Tsigaridis, K., Tselioudis, G., Weng, E., Wu, J., and
 1546 Yao, M.-S.: GISS-E2.1: Configurations and Climatology, *Journal of Advances in Modeling*
 1547 *Earth Systems*, 12, e2019MS002025, <https://doi.org/10.1029/2019MS002025>, 2020.
 1548 Kim, Y., Moorcroft, P. R., Aleinov, I., Puma, M. J., and Kiang, N. Y.: Variability of phenology
 1549 and fluxes of water and carbon with observed and simulated soil moisture in the Ent
 1550 Terrestrial Biosphere Model (Ent TBM version 1.0.1.0.0), 8, 3837–3865,
 1551 <https://doi.org/10.5194/gmd-8-3837-2015>, 2015.
 1552 Kyker-Snowman, E., Lombardozi, D. L., Bonan, G. B., Cheng, S. J., Dukes, J. S., Frey, S. D.,
 1553 Jacobs, E. M., McNellis, R., Rady, J. M., Smith, N. G., Thomas, R. Q., Wieder, W. R., and
 1554 Grandy, A. S.: Increasing the spatial and temporal impact of ecological research: A
 1555 roadmap for integrating a novel terrestrial process into an Earth system model, 28, 665–
 1556 684, <https://doi.org/10.1111/gcb.15894>, 2022.
 1557 Litton, C. M., Raich, J. W., and Ryan, M. G.: Carbon allocation in forest ecosystems, *Global*
 1558 *Change Biol*, 13, 2089–2109, <https://doi.org/10.1111/j.1365-2486.2007.01420.x>, 2007.
 1559 Liu, H., Gleason, S. M., Hao, G., Hua, L., He, P., Goldstein, G., and Ye, Q.: Hydraulic traits are
 1560 coordinated with maximum plant height at the global scale, 5, eaav1332,
 1561 <https://doi.org/10.1126/sciadv.aav1332>, 2019.
 1562 Lloret, F., Escudero, A., Iriondo, J. M., Martínez-Vilalta, J., and Valladares, F.: Extreme climatic
 1563 events and vegetation: the role of stabilizing processes, 18, 797–805,
 1564 <https://doi.org/10.1111/j.1365-2486.2011.02624.x>, 2012.
 1565 Lu, R., Qiao, Y., Wang, J., Zhu, C., Cui, E., Xu, X., He, Y., Zhao, Z., Du, Y., Yan, L., Shen, G.,
 1566 Yang, Q., Wang, X., and Xia, J.: The U-shaped pattern of size-dependent mortality and its
 1567 correlated factors in a subtropical monsoon evergreen forest, 109, 2421–2433,
 1568 <https://doi.org/10.1111/1365-2745.13652>, 2021.
 1569 Luo, Y., Weng, E., Wu, X., Gao, C., Zhou, X., and Zhang, L.: Parameter identifiability,
 1570 constraint, and equifinality in data assimilation with ecosystem models, 19, 571–574,
 1571 <https://doi.org/10.1890/08-0561.1>, 2009.
 1572 MacBean, N., Peylin, P., Chevallier, F., Scholze, M., and Schuermann, G.: Consistent
 1573 assimilation of multiple data streams in a carbon cycle data assimilation system, 9, 3569–
 1574 3588, <https://doi.org/10.5194/gmd-9-3569-2016>, 2016.
 1575 Manzoni, S., Trofymow, J. A., Jackson, R. B., and Porporato, A.: Stoichiometric controls on
 1576 carbon, nitrogen, and phosphorus dynamics in decomposing litter, 80, 89–106, 2010.
 1577 Manzoni, S., Vico, G., Thompson, S., Beyer, F., and Weih, M.: Contrasting leaf phenological
 1578 strategies optimize carbon gain under droughts of different duration, *Advances in Water*
 1579 *Resources*, 84, 37–51, <https://doi.org/10.1016/j.advwatres.2015.08.001>, 2015.
 1580 McDowell, N. G.: Mechanisms Linking Drought, Hydraulics, Carbon Metabolism, and
 1581 Vegetation Mortality, 155, 1051–1059, <https://doi.org/10.1104/pp.110.170704>, 2011.

1582 McDowell, N. G., Allen, C. D., Anderson-Teixeira, K., Aukema, B. H., Bond-Lamberty, B.,
 1583 Chini, L., Clark, J. S., Dietze, M., Grossiord, C., Hanbury-Brown, A., Hurtt, G. C.,
 1584 Jackson, R. B., Johnson, D. J., Kueppers, L., Lichstein, J. W., Ogle, K., Poulter, B., Pugh,
 1585 T. A. M., Seidl, R., Turner, M. G., Uriarte, M., Walker, A. P., and Xu, C.: Pervasive shifts
 1586 in forest dynamics in a changing world, 368, <https://doi.org/10.1126/science.aaz9463>,
 1587 2020.

1588 McNickle, G. G., Gonzalez-Meler, M. A., Lynch, D. J., Baltzer, J. L., and Brown, J. S.: The
 1589 world's biomes and primary production as a triple tragedy of the commons foraging game
 1590 played among plants, 283, 20161993, <https://doi.org/10.1098/rspb.2016.1993>, 2016.

1591 Meir, P., Cox, P., and Grace, J.: The influence of terrestrial ecosystems on climate, *Trends in*
 1592 *Ecology & Evolution*, 21, 254–260, <https://doi.org/10.1016/j.tree.2006.03.005>, 2006.

1593 van der Molen, M. K., Dolman, A. J., Ciais, P., Eglin, T., Gobron, N., Law, B. E., Meir, P.,
 1594 Peters, W., Phillips, O. L., Reichstein, M., Chen, T., Dekker, S. C., Doubkova, M., Friedl,
 1595 M. A., Jung, M., van den Hurk, B. J. J. M., de Jeu, R. A. M., Kruijt, B., Ohta, T., Rebel, K.
 1596 T., Plummer, S., Seneviratne, S. I., Sitch, S., Teuling, A. J., van der Werf, G. R., and
 1597 Wang, G.: Drought and ecosystem carbon cycling, *Agricultural and Forest Meteorology*,
 1598 151, 765–773, <https://doi.org/10.1016/j.agrformet.2011.01.018>, 2011.

1599 Montané, F., Fox, A. M., Arellano, A. F., MacBean, N., Alexander, M. R., Dye, A., Bishop, D.
 1600 A., Trouet, V., Babst, F., Hessler, A. E., Pederson, N., Blanken, P. D., Bohrer, G., Gough, C.
 1601 M., Litvak, M. E., Novick, K. A., Phillips, R. P., Wood, J. D., and Moore, D. J. P.:
 1602 Evaluating the effect of alternative carbon allocation schemes in a land surface model
 1603 (CLM4.5) on carbon fluxes, pools, and turnover in temperate forests, 10, 3499–3517,
 1604 <https://doi.org/10.5194/gmd-10-3499-2017>, 2017.

1605 Niinemets, Ü. and Anten, N. P. R.: Packing the Photosynthetic Machinery: From Leaf to
 1606 Canopy, in: *Photosynthesis in silico: Understanding Complexity from Molecules to*
 1607 *Ecosystems*, edited by: Laisk, A., Nedbal, L., and Govindjee, Springer Netherlands,
 1608 Dordrecht, 363–399, https://doi.org/10.1007/978-1-4020-9237-4_16, 2009.

1609 Niinemets, Ü., Keenan, T. F., and Hallik, L.: A worldwide analysis of within-canopy variations
 1610 in leaf structural, chemical and physiological traits across plant functional types, 205, 973–
 1611 993, <https://doi.org/10.1111/nph.13096>, 2015.

1612 Niklas, K.: Plant Height and the Properties of Some Herbaceous Stems, 75, 133–142,
 1613 <https://doi.org/10.1006/anbo.1995.1004>, 1995.

1614 Nobre, C. A., Sellers, P. J., and Shukla, J.: Amazonian Deforestation and Regional Climate
 1615 Change, *J. Climate*, 4, 957–988, [https://doi.org/10.1175/1520-0442\(1991\)004<0957:ADARCC>2.0.CO;2](https://doi.org/10.1175/1520-0442(1991)004<0957:ADARCC>2.0.CO;2), 1991.

1617 Oliveira, R. S., Eller, C. B., Barros, F. de V., Hirota, M., Brum, M., and Bittencourt, P.: Linking
 1618 plant hydraulics and the fast–slow continuum to understand resilience to drought in tropical
 1619 ecosystems, 230, 904–923, <https://doi.org/10.1111/nph.17266>, 2021.

1620 Osnas, J. L. D., Lichstein, J. W., Reich, P. B., and Pacala, S. W.: Global Leaf Trait
 1621 Relationships: Mass, Area, and the Leaf Economics Spectrum, 340, 741–744,
 1622 <https://doi.org/10.1126/science.1231574>, 2013.

- 1623 Pan, Y., Birdsey, R. A., Phillips, O. L., and Jackson, R. B.: The Structure, Distribution, and
1624 Biomass of the World's Forests, 44, 593–622, [https://doi.org/10.1146/annurev-ecolsys-](https://doi.org/10.1146/annurev-ecolsys-110512-135914)
1625 110512-135914, 2013.
- 1626 Pavlick, R., Drewry, D. T., Bohn, K., Reu, B., and Kleidon, A.: The Jena Diversity-Dynamic
1627 Global Vegetation Model (JeDi-DGVM): a diverse approach to representing terrestrial
1628 biogeography and biogeochemistry based on plant functional trade-offs, 10, 4137–4177,
1629 <https://doi.org/10.5194/bg-10-4137-2013>, 2013.
- 1630 Pielke, R. A., Sr., ., Avissar, RonI., Raupach, M., Dolman, A. J., Zeng, X., and Denning, A. S.:
1631 Interactions between the atmosphere and terrestrial ecosystems: influence on weather and
1632 climate, 4, 461–475, <https://doi.org/10.1046/j.1365-2486.1998.t01-1-00176.x>, 1998.
- 1633 Potter, C., Klooster, S., Myneni, R., Genovese, V., Tan, P., and Kumar, V.: Continental-scale
1634 comparisons of terrestrial carbon sinks estimated from satellite data and ecosystem
1635 modeling 1982–1998, 39, 201–213, <https://doi.org/10.1016/j.gloplacha.2003.07.001>, 2003.
- 1636 Potter, C. S., Randerson, J. T., Field, C. B., Matson, P. A., Vitousek, P. M., Mooney, H. A., and
1637 Klooster, S. A.: Terrestrial ecosystem production: A process model based on global
1638 satellite and surface data, 7, 811–841, <https://doi.org/10.1029/93GB02725>, 1993.
- 1639 Powell, T. L., Galbraith, D. R., Christoffersen, B. O., Harper, A., Imbuzeiro, H. M. A., Rowland,
1640 L., Almeida, S., Brando, P. M., da Costa, A. C. L., Costa, M. H., Levine, N. M., Malhi, Y.,
1641 Saleska, S. R., Sotta, E., Williams, M., Meir, P., and Moorcroft, P. R.: Confronting model
1642 predictions of carbon fluxes with measurements of Amazon forests subjected to
1643 experimental drought, 200, 350–365, <https://doi.org/10.1111/nph.12390>, 2013.
- 1644 Prentice, I. C., Cramer, W., Harrison, S. P., LEEMANS, R., Monserud, R. A., and Solomon, A.
1645 M.: A global biome model based on plant physiology and dominance, soil properties and
1646 climate, 19, 117–134, <https://doi.org/10.2307/2845499>, 1992.
- 1647 Prentice, I. C., Bondeau, A., Cramer, W., Harrison, S. P., Hickler, T., Lucht, W., Sitch, S., Smith,
1648 B., and Sykes, M. T.: Dynamic Global Vegetation Modeling: Quantifying Terrestrial
1649 Ecosystem Responses to Large-Scale Environmental Change, in: *Terrestrial Ecosystems in
1650 a Changing World*, edited by: Canadell, J. G., Pataki, D. E., and Pitelka, L. F., Springer
1651 Berlin Heidelberg, Berlin, Heidelberg, 175–192, [https://doi.org/10.1007/978-3-540-32730-](https://doi.org/10.1007/978-3-540-32730-1_15)
1652 1_15, 2007.
- 1653 Prentice, I. C., Dong, N., Gleason, S. M., Maire, V., and Wright, I. J.: Balancing the costs of
1654 carbon gain and water transport: testing a new theoretical framework for plant functional
1655 ecology, 17, 82–91, <https://doi.org/10.1111/ele.12211>, 2014.
- 1656 Purves, D. and Pacala, S.: Predictive models of forest dynamics, 320, 1452–1453,
1657 <https://doi.org/10.1126/science.1155359>, 2008.
- 1658 Purves, D. W., Lichstein, J. W., Strigul, N., and Pacala, S. W.: Predicting and understanding
1659 forest dynamics using a simple tractable model, 105, 17018–17022,
1660 <https://doi.org/10.1073/pnas.0807754105>, 2008.
- 1661 Randerson, J., Thompson, M., Conway, T., Fung, I., and Field, C.: The contribution of terrestrial
1662 sources and sinks to trends in the seasonal cycle of atmospheric carbon dioxide, 11, 535–
1663 560, <https://doi.org/10.1029/97GB02268>, 1997.

1664 Reich, P. B.: The world-wide ‘fast–slow’ plant economics spectrum: a traits manifesto, 102,
1665 275–301, <https://doi.org/10.1111/1365-2745.12211>, 2014.

1666 Reyser, C. P. O., Leuzinger, S., Rammig, A., Wolf, A., Bartholomeus, R. P., Bonfante, A., de
1667 Lorenzi, F., Dury, M., Gloning, P., Abou Jaoudé, R., Klein, T., Kuster, T. M., Martins, M.,
1668 Niedrist, G., Riccardi, M., Wohlfahrt, G., de Angelis, P., de Dato, G., François, L., Menzel,
1669 A., and Pereira, M.: A plant’s perspective of extremes: terrestrial plant responses to
1670 changing climatic variability, 19, 75–89, <https://doi.org/10.1111/gcb.12023>, 2013.

1671 Rodriguez-Iturbe, I., Porporato, A., Ridolfi, L., Isham, V., and Cox, D. R.: Probabilistic
1672 modelling of water balance at a point: the role of climate, soil and vegetation, 455, 3789–
1673 3805, <https://doi.org/10.1098/rspa.1999.0477>, 1999.

1674 Rosenzweig, C. and Abramopoulos, F.: Land-Surface Model Development for the GISS GCM,
1675 10, 2040–2054, [https://doi.org/10.1175/1520-0442\(1997\)010<2040:LSMDFT>2.0.CO;2](https://doi.org/10.1175/1520-0442(1997)010<2040:LSMDFT>2.0.CO;2),
1676 1997.

1677 Scheiter, S., Langan, L., and Higgins, S. I.: Next-generation dynamic global vegetation models:
1678 learning from community ecology, 198, 957–969, <https://doi.org/10.1111/nph.12210>, 2013.

1679 Schmidt, G. A., Kelley, M., Nazarenko, L., Ruedy, R., Russell, G. L., Aleinov, I., Bauer, M.,
1680 Bauer, S. E., Bhat, M. K., Bleck, R., Canuto, V., Chen, Y.-H., Cheng, Y., Clune, T. L., Del
1681 Genio, A., de Fainchtein, R., Faluvegi, G., Hansen, J. E., Healy, R. J., Kiang, N. Y., Koch,
1682 D., Lacis, A. A., LeGrande, A. N., Lerner, J., Lo, K. K., Matthews, E. E., Menon, S.,
1683 Miller, R. L., Oinas, V., Olos, A. O., Perlwitz, J. P., Puma, M. J., Putman, W. M., Rind,
1684 D., Romanou, A., Sato, M., Shindell, D. T., Sun, S., Syed, R. A., Tausnev, N., Tsigaridis,
1685 K., Unger, N., Voulgarakis, A., Yao, M.-S., and Zhang, J.: Configuration and assessment of
1686 the GISS ModelE2 contributions to the CMIP5 archive, 6, 141–184,
1687 <https://doi.org/10.1002/2013MS000265>, 2014.

1688 Sellers, P. J.: Modeling the Exchanges of Energy, Water, and Carbon Between Continents and
1689 the Atmosphere, 275, 502–509, <https://doi.org/10.1126/science.275.5299.502>, 1997.

1690 Simard, M., Pinto, N., Fisher, J. B., and Baccini, A.: Mapping forest canopy height globally with
1691 spaceborne lidar, 116, <https://doi.org/10.1029/2011JG001708>, 2011.

1692 Singh, A. K., Dhanapal, S., and Yadav, B. S.: The dynamic responses of plant physiology and
1693 metabolism during environmental stress progression, *Mol Biol Rep*, 47, 1459–1470,
1694 <https://doi.org/10.1007/s11033-019-05198-4>, 2020.

1695 Sitch, S., Smith, B., Prentice, I. C., Arneth, A., Bondeau, A., Cramer, W., Kaplan, J. O., Levis,
1696 S., Lucht, W., Sykes, M. T., Thonicke, K., and Venevsky, S.: Evaluation of ecosystem
1697 dynamics, plant geography and terrestrial carbon cycling in the LPJ dynamic global
1698 vegetation model, 9, 161–185, <https://doi.org/10.1046/j.1365-2486.2003.00569.x>, 2003.

1699 Sitch, S., Friedlingstein, P., Gruber, N., Jones, S. D., Murray-Tortarolo, G., Ahlström, A.,
1700 Doney, S. C., Graven, H., Heinze, C., Huntingford, C., Levis, S., Levy, P. E., Lomas, M.,
1701 Poulter, B., Viovy, N., Zaehle, S., Zeng, N., Arneth, A., Bonan, G., Bopp, L., Canadell, J.
1702 G., Chevallier, F., Ciais, P., Ellis, R., Gloor, M., Peylin, P., Piao, S. L., Le Quéré, C.,
1703 Smith, B., Zhu, Z., and Myneni, R.: Recent trends and drivers of regional sources and sinks
1704 of carbon dioxide, *Biogeosciences*, 12, 653–679, <https://doi.org/10.5194/bg-12-653-2015>,
1705 2015.

1706 Strigul, N., Pristinski, D., Purves, D., Dushoff, J., and Pacala, S.: Scaling from trees to forests:
1707 tractable macroscopic equations for forest dynamics, 78, 523–545,
1708 <https://doi.org/10.1890/08-0082.1>, 2008.

1709 Swenson, N. G. and Enquist, B. J.: Ecological and evolutionary determinants of a key plant
1710 functional trait: wood density and its community-wide variation across latitude and
1711 elevation, 94, 451–459, <https://doi.org/10.3732/ajb.94.3.451>, 2007.

1712 Tifafi, M., Guenet, B., and Hatté, C.: Large Differences in Global and Regional Total Soil
1713 Carbon Stock Estimates Based on SoilGrids, HWSD, and NCSCD: Intercomparison and
1714 Evaluation Based on Field Data From USA, England, Wales, and France, 32, 42–56,
1715 <https://doi.org/10.1002/2017GB005678>, 2018.

1716 Tilman, D.: Plant strategies and the dynamics and structure of plant communities, Princeton
1717 University Press, Princeton, N.J, 360 pp., 1988.

1718 Verryckt, L. T., Vicca, S., Van Langenhove, L., Stahl, C., Asensio, D., Urbina, I., Ogaya, R.,
1719 Llusà, J., Grau, O., Peguero, G., Gargallo-Garriga, A., Courtois, E. A., Margalef, O.,
1720 Portillo-Estrada, M., Ciais, P., Obersteiner, M., Fuchslueger, L., Lugli, L. F., Fernandez-
1721 Garberí, P.-R., Vallicrosa, H., Verlinden, M., Ranits, C., Vermeir, P., Coste, S.,
1722 Verbruggen, E., Bréchet, L., Sardans, J., Chave, J., Peñuelas, J., and Janssens, I. A.:
1723 Vertical profiles of leaf photosynthesis and leaf traits and soil nutrients in two tropical
1724 rainforests in French Guiana before and after a 3-year nitrogen and phosphorus addition
1725 experiment, 14, 5–18, <https://doi.org/10.5194/essd-14-5-2022>, 2022.

1726 Volaire, F.: A unified framework of plant adaptive strategies to drought: Crossing scales and
1727 disciplines, 24, 2929–2938, <https://doi.org/10.1111/gcb.14062>, 2018.

1728 Wang, H., Prentice, I. C., Keenan, T. F., Davis, T. W., Wright, I. J., Cornwell, W. K., Evans, B.
1729 J., and Peng, C.: Towards a universal model for carbon dioxide uptake by plants, 3, 734–
1730 741, <https://doi.org/10.1038/s41477-017-0006-8>, 2017.

1731 Wang, Y.-P. and Goll, D. S.: Modelling of land nutrient cycles: recent progress and future
1732 development, *Fac Rev*, 10, 53, <https://doi.org/10.12703/r/10-53>, 2021.

1733 Wang, Y.-P., Trudinger, C. M., and Enting, I. G.: A review of applications of model–data fusion
1734 to studies of terrestrial carbon fluxes at different scales, 149, 1829–1842,
1735 <https://doi.org/10.1016/j.agrformet.2009.07.009>, 2009.

1736 Wei, N., Xia, J., Zhou, J., Jiang, L., Cui, E., Ping, J., and Luo, Y.: Evolution of Uncertainty in
1737 Terrestrial Carbon Storage in Earth System Models from CMIP5 to CMIP6, 1, 1–33,
1738 <https://doi.org/10.1175/JCLI-D-21-0763.1>, 2022.

1739 Weng, E. and Luo, Y.: Relative information contributions of model vs. data to short- and long-
1740 term forecasts of forest carbon dynamics, 21, 1490–1505, 2011.

1741 Weng, E., Luo, Y., Gao, C., and Oren, R.: Uncertainty analysis of forest carbon sink forecast
1742 with varying measurement errors: a data assimilation approach, 4, 178–191,
1743 <https://doi.org/10.1093/jpe/rtr018>, 2011.

1744 Weng, E., Farrior, C. E., Dybzinski, R., and Pacala, S. W.: Predicting vegetation type through
1745 physiological and environmental interactions with leaf traits: evergreen and deciduous

1746 forests in an earth system modeling framework, 23, 2482–2498,
 1747 <https://doi.org/10.1111/gcb.13542>, 2017.

1748 Weng, E., Dybzinski, R., Farrior, C. E., and Pacala, S. W.: Competition alters predicted forest
 1749 carbon cycle responses to nitrogen availability and elevated CO₂: simulations using an
 1750 explicitly competitive, game-theoretic vegetation demographic model, 16, 4577–4599,
 1751 <https://doi.org/10.5194/bg-16-4577-2019>, 2019.

1752 Weng, E. S., Malyshev, S., Lichstein, J. W., Farrior, C. E., Dybzinski, R., Zhang, T.,
 1753 Shevliakova, E., and Pacala, S. W.: Scaling from individual trees to forests in an Earth
 1754 system modeling framework using a mathematically tractable model of height-structured
 1755 competition, 12, 2655–2694, <https://doi.org/10.5194/bg-12-2655-2015>, 2015.

1756 Wieder, W. R., Grandy, A. S., Kallenbach, C. M., and Bonan, G. B.: Integrating microbial
 1757 physiology and physio-chemical principles in soils with the Microbial-MIneral Carbon
 1758 Stabilization (MIMICS) model, 11, 3899–3917, <https://doi.org/10.5194/bg-11-3899-2014>,
 1759 2014.

1760 Williams, M., Richardson, A. D., Reichstein, M., Stoy, P. C., Peylin, P., Verbeeck, H.,
 1761 Carvalhais, N., Jung, M., Hollinger, D. Y., Kattge, J., Leuning, R., Luo, Y., Tomelleri, E.,
 1762 Trudinger, C. M., and Wang, Y.-P.: Improving land surface models with FLUXNET data,
 1763 *Biogeosciences*, 6, 1341–1359, <https://doi.org/10.5194/bg-6-1341-2009>, 2009.

1764 Woodward, F. I., Lomas, M. R., and Betts, R. A.: Vegetation-climate feedbacks in a greenhouse
 1765 world, *Phil. Trans. R. Soc. Lond. B*, 353, 29–39, <https://doi.org/10.1098/rstb.1998.0188>,
 1766 1998.

1767 Xia, J., Luo, Y., Wang, Y.-P., and Hararuk, O.: Traceable components of terrestrial carbon
 1768 storage capacity in biogeochemical models, 19, 2104–2116,
 1769 <https://doi.org/10.1111/gcb.12172>, 2013.

1770 Xia, J., Yuan, W., Wang, Y.-P., and Zhang, Q.: Adaptive Carbon Allocation by Plants Enhances
 1771 the Terrestrial Carbon Sink, *Sci Rep*, 7, 3341, <https://doi.org/10.1038/s41598-017-03574-3>,
 1772 2017.

1773 Xia, J., Yuan, W., Lienert, S., Joos, F., Ciais, P., Viovy, N., Wang, Y., Wang, X., Zhang, H.,
 1774 Chen, Y., and Tian, X.: Global Patterns in Net Primary Production Allocation Regulated by
 1775 Environmental Conditions and Forest Stand Age: A Model-Data Comparison, 124, 2039–
 1776 2059, <https://doi.org/10.1029/2018JG004777>, 2019.

1777 Xu, T., White, L., Hui, D., and Luo, Y.: Probabilistic inversion of a terrestrial ecosystem model:
 1778 Analysis of uncertainty in parameter estimation and model prediction, 20, GB2007,
 1779 <https://doi.org/10.1029/2005GB002468>, 2006.

1780 Yizhao, C., Jianyang, X., Zhengguo, S., Jianlong, L., Yiqi, L., Chengcheng, G., and Zhaoqi, W.:
 1781 The role of residence time in diagnostic models of global carbon storage capacity: model
 1782 decomposition based on a traceable scheme, *Sci Rep*, 5, 16155,
 1783 <https://doi.org/10.1038/srep16155>, 2015.

1784 Yuan, W., Luo, Y., Liang, S., Yu, G., Niu, S., Stoy, P., Chen, J., Desai, A. R., Lindroth, A.,
 1785 Gough, C. M., Ceulemans, R., Arain, A., Bernhofer, C., Cook, B., Cook, D. R., Dragoni,
 1786 D., Gielen, B., Janssens, I. A., Longdoz, B., Liu, H., Lund, M., Matteucci, G., Moors, E.,

1787 Scott, R. L., Seufert, G., and Varner, R.: Thermal adaptation of net ecosystem exchange, 8,
1788 1453–1463, <https://doi.org/10.5194/bg-8-1453-2011>, 2011.

1789 Zeng, Z., Piao, S., Li, L. Z. X., Zhou, L., Ciais, P., Wang, T., Li, Y., Lian, X., Wood, E. F.,
1790 Friedlingstein, P., Mao, J., Estes, L. D., Myneni, R. B., Peng, S., Shi, X., Seneviratne, S. I.,
1791 and Wang, Y.: Climate mitigation from vegetation biophysical feedbacks during the past
1792 three decades, 7, 432–436, <https://doi.org/10.1038/nclimate3299>, 2017.

1793 Zhou, G., Houlton, B. Z., Wang, W., Huang, W., Xiao, Y., Zhang, Q., Liu, S., Cao, M., Wang,
1794 X., Wang, S., Zhang, Y., Yan, J., Liu, J., Tang, X., and Zhang, D.: Substantial
1795 reorganization of China’s tropical and subtropical forests: based on the permanent plots,
1796 20, 240–250, <https://doi.org/10.1111/gcb.12385>, 2014.

1797 Zhou, J., Xia, J., Wei, N., Liu, Y., Bian, C., Bai, Y., and Luo, Y.: A traceability analysis system
1798 for model evaluation on land carbon dynamics: design and applications, *Ecol Process*, 10,
1799 12, <https://doi.org/10.1186/s13717-021-00281-w>, 2021.

1800 Zuleta, D., Arellano, G., Muller-Landau, H. C., McMahon, S. M., Aguilar, S., Bunyavejchewin,
1801 S., Cárdenas, D., Chang-Yang, C.-H., Duque, A., Mitre, D., Nasardin, M., Pérez, R., Sun,
1802 I.-F., Yao, T. L., and Davies, S. J.: Individual tree damage dominates mortality risk factors
1803 across six tropical forests, 233, 705–721, <https://doi.org/10.1111/nph.17832>, 2022.

1804

Page 10: [1] Deleted 10:42:00 AM	Weng, Ensheng (GISS-6110)[TRUSTEES OF COLUMBIA UNIVERSITY]	6/15/22
-------------------------------------	------------------------------------------------------------	---------

Page 15: [2] Deleted 6:29:00 PM	Weng, Ensheng (GISS-6110)[TRUSTEES OF COLUMBIA UNIVERSITY]	6/16/22
------------------------------------	------------------------------------------------------------	---------